Journal Name : EASTERN ANATOLIAN JOURNAL OF SCIENCE

Managing Office : Ağrı İbrahim Çeçen University

Web Site : http://www.agri.edu.tr/tr/e-dergiler/eajs

http://dergipark.ulakbim.gov.tr/eajs/

E-Mail : eajs@agri.edu.tr

Managing Office Tel : +90 472 215 50 82

Publication Language : English

Publication Type : International Journal

Online Published : November, 2017

PREFACE

Dear scientist,

I am happy to announce that Volume III - Issue II of the Eastern Anatolian Journal of Science (EAJS) has been published. This issue is composed of 5 original papers that possess some of the leading and advanced techniques of natural and applied sciences. On behalf of the owner of EAJS, I would like to thank all authors, referees, our editorial board members and section editors that provide valuable contributions for the publication of the issue.

EAJS will publish original and high-quality articles covering a wide range of topics in scientific research, dedicated to promoting high standards and excellence in the creation and dissemination of scientific knowledge. EAJS published in English is open access journal and abstracting and indexing by various international index services.

Authors are solicited to contribute to the EAJS by submitting articles that illustrate research results, projects, surveying works and industrial experiences that describe significant advances in the following areas, but are not limited to:

- Biology
- Chemistry
- Engineering
- Mathematics
- Nanoscience and Nanotechnology
- Physics

Our previous issues have an attraction in terms of scientific quality and impact factor of articles by favorable feedbacks of readers. Our editorial team lend wings to be an internationally reputable and pioneer journal of science by their outstanding scientific personality. I am hoping to work effectively with our editorial team in the future.

I'd like to express my gratitude to all authors, members of editorial board and contributing reviewers. My sincere thanks go to Prof. Dr. Abdulhalik KARABULUT, the rector of Ağrı İbrahim Çeçen University, sets the goal of being also a top-ranking university in scientific sense, for supporting and motivating us in every respect. I express my gratitude to the members of technical staff of the journal for the design and proofreading of the articles. Last but not least, my special thanks go to the respectable businessman Mr. İbrahim ÇEÇEN who unsparingly supports our university financially and emotionally, to his team and to the director and staff of IC foundation.

I invite scientists from all branches of science to contribute our journal by sending papers for publication in EAJS.

Assoc. Prof. Dr. İbrahim HAN

Editor-in-Chief

CONTENTS

YBa2Cu3O7-δ Thin Film Growth on Different Substrates by Pulsed Laser Deposition 1-7

By M. T. YURTCAN, Ö. ŞİMŞEK, Ö. BAYRAM and M. ERTUĞRUL

Phenomenological and Microscopic Analysis of Elastic Scattering Reactions of ^{20}Ne by ^{12}C, ^{16}O, ^{28}Si, ^{58}Ni 8-15

By M. AYGÜN

Performance Analysis of Speed Control of PMDC Motor using Fuzzy Logic Controller 16-29

By M. R. ÇORAPSIZ

Chemometric Analysis of Moxifloxacin and Metronidazole in Binary Drug Combinations With Spectrophotometric Method 30-37

By G. P. ERTOKUŞ and Ü. M. ÇELİK

Evaluation of Detection Limits with Wavelength Dispersive X-Ray Fluorescence Spectrometry 38-47

By E. S. ÜNAL and N. EKİNCİ

$YBa_2Cu_3O_{7-\delta}$ Thin Film Growth on Different Substrates by Pulsed Laser Deposition

MUSTAFA TOLGA YURTCAN*[1, 2], ÖNDER ŞİMŞEK[1, 2], ÖZKAN BAYRAM[3], MEHMET ERTUĞRUL[1, 4]

[1]Atatürk University, Department of Nanoscience and Nanoengineering, Erzurum, TURKEY
[2]Atatürk University, Department of Physics Education, Erzurum, TURKEY
[3]Bayburt University, Department of Materials Science and Nanotechnology Engineering, Bayburt, TURKEY
[4]Atatürk University, Department of Electrical and Electronics Engineering, Erzurum, TURKEY

Abstract

There were a lot of research on $YBa_2Cu_3O_{7-\delta}$ (YBCO) superconducting materials and this material still draw attention. In this research, thin films of commonly used superconducting YBCO ceramic material, grown on $LaAlO_3$ (LAO), MgO and $SrTiO_3$ (STO) substrates as thin films, which have different thermal expansion constants and lattice parameters, by Pulsed Laser Deposition (PLD) technique. 150 mTorr partial Oxygen pressure, 5 cm substrate to target distance and 800 °C substrate temperature used for all thin film growths. Thin films characterized for film quality and microstructure with X-Ray Diffraction (XRD), Scanning Electron Microscopy (SEM) and Energy Dispersive Spectroscopy (EDS) techniques. Analysis of these thin films showed that highly *c* oriented *(00l)* YBCO thin films obtained with LAO and STO substrates, which are more compatible than MgO for YBCO growth.

Keywords: $YBa_2Cu_3O_{7-\delta}$ thin films, YBCO, $LaAlO_3$, MgO, $SrTiO_3$, Superconductivity, Pulsed Laser Deposition, PLD

1. Introduction

Superconducting materials show almost zero resistance under a critical temperature and commonly used for high magnetic field generation, magnetic levitation, electric transport and magnetic imaging systems. YBCO material contains Yttrium, Barium, Cupper and Oxygen elements in its structure with oxygen deficiency and it is a very important Type-2 high temperature superconductor. YBCO shows superconductivity at 93 K which is over the boiling point of liquid Nitrogen (77 K) (Wu *et al.* 1987). YBCO ceramic has a three-layered perovskite structure without any toxic or volatile components. YBCO crystal in orthorhombic structure has superconducting properties with lattice parameters of a = 3.82 Å, b = 3.89 Å and c = 11.67 Å (Kim and Lee 1999). Thermal expansion constant of YBCO is given as 13.4 $x10^{-6}$ $°C^{-1}$ (Kawashima *et al.* 1998). Thin films of YBCO finds usage in micro-electronic devices such as detector and filters (Li *et al.* 2017), especially as Superconducting QUantum Interference Devices (SQUIDs) for magnetic flux change detection (Lee *et al.* 1995) and bolometers for electromagnetic radiation detection (Aboudihab *et al.* 1994). It is possible to grow thin films on many different substrates, but for a selective directional crystal growth, it is essential to choose a substrate with lattice match and similar thermal expansion constants, without any chemical reaction between substrate and deposition material. Substrate selection is very important for high quality superconducting thin films, suitable for device applications. Substrate effect should not be ignored, since it has significant role in determination of the properties of the thin film it supports and specific applications require various substrates for different purposes (Phillips 1996).

Pulsed Laser Deposition (PLD) is a favored physical vapor deposition technique used for growth of high quality single crystal thin and thick films of one element to complex structures (Lee *et al.* 1991; Bierleutgeb and Proyer 1997). This technique has many variables that affect the film growth substantially. (Chrisey and Hubler 1994; Proyer and Stangl 1995; Proyer *et al.* 1996). In order to obtain a good film, variables like; spot size, laser energy, deposition pressure, deposition gas, number of pulses, pulse frequency, heating and cooling rates, target rotation and raster speeds, substrate rotation speed and substrate to target distance has to be optimized (Chrisey and Hubler 1994; Duhalde *et al.* 1998; Kim and Lee 1999). It is

Received: 31.07.2017
Revised: 10.08.2017
Accepted: 28.09.2017
Corresponding author: Mustafa Tolga Yurtcan, PhD
Atatürk University, Department of Nanoscience and Nanoengineering, Erzurum, Turkey
E-mail: yurtcan@atauni.edu.tr
Cite this article as: M. T. Yurtcan, Ö. Şimşek, Ö. Bayram, and M. Ertuğrul,$YBa_2Cu_3O_{7-\delta}$ Thin Film Growth on Different Substrates by Pulsed Laser Deposition, Eastern Anatolian Journal of Science, Vol. 3, Issue 2, 1-7, 2017.

possible to grow sandwich structures with multiple target holders by PLD. Contaminations can be prevented with in-situ annealing of the samples inside the PLD chamber.

In this study, previously optimized YBCO thin film growth parameters (Yurtcan *et al.* 2013) were used for growth of the YBCO thin films on 3 various substrates; $LaAlO_3$ (LAO), MgO and $SrTiO_3$ (STO) having different lattice parameters. Thin films of YBCO on different substrates characterized and best thin film that is closest to single crystal for device applications was determined.

2. Experimental Details

All of the substrate materials for YBCO growth purchased from MTI Corporation as wafers and sliced substrates. Wafers and substrates were 1 side polished and (*100)* oriented single crystals. LAO sliced from 3 inch diameter wafer into 15 x 5 mm substrates with a diamond saw in our laboratory. MgO sliced from 2 inch side length square wafer into 10 x 10 mm square substrates with a Disco DAD322 Automatic Dicing Saw in East Anatolia High Technology Application and Research Center (DAYTAM). STO substrates purchased as 10 x 10 mm square substrates and used as they were. Table.1 shows the lattice parameters, dielectric and thermal expansion constants of these substrates.

Table.1. Physical properties of the substrates.

	Lattice Parameters	Dielectric Constant	Thermal Expansion Constant
LAO	a = b = 3.790 Å	~ 25	10 x10^{-6} °C^{-1}
MgO	a = b = 4.216 Å	9.8	12.8 x10^{-6} °C^{-1}
STO	a = b = 3.905 Å	~ 300	10.4 x10^{-6} °C^{-1}

Compared to MgO's lattice, LAO and STO lattice parameters are very close to YBCO's *a* and *b* values. On the other hand, thermal expansion constant of MgO is more compatible than LAO and STO for YBCO thin films.

Prior to the substrate pasting into substrate holder, all the substrates cleaned with acetone and methanol for 8 minutes in an ultrasonic bath to prevent organic contamination on substrate surfaces. Cleaned substrates pasted into substrate holder with Ted Pella Inc. Leitsilber 200 Silver Paint and then left for drying about 30 minutes.

YBCO target prepared by cold pressing 9.5 grams of high purity YBCO powder (Matech Inc.) with a density of 6.30 g/cm^3 into 1 inch die set. YBCO pellet than sintered at 905 °C for 20 hours in atmosphere for hardening (Yanmaz *et al.* 2009).

Thin films grown by Neocera Inc. "Complete P180 PLD Laboratory" system with a 248 nm wavelength KrF excimer laser "Coherent Compex Pro 102" in Atatürk University. Fixed growth parameters were 5 cm substrate to target distance, 150 mTorr O_2 partial pressure, 800 °C substrate temperature and 10 Hz frequency. (Yurtcan 2011; Yurtcan *et al.* 2013). Vacuum chamber evacuated by a turbo molecular pump in order to prevent contamination of thin films during growth. Substrates heated to 800 °C and the chamber pressure increased to 150 mTorr with 99.999% high purity O_2 gas by a mass flow controller. Prior to crystal growth, a shutter used to cover the substrate and laser fired upon YBCO target to clean target surface. After that, shutter opened and 6000 laser pulses used for crystal growth. As soon as crystal growth finished O_2 gas flow switched off and substrate temperature reduced to 400 °C with 10 °C/min ramp rate to prevent cracking between substrate and the thin film. When the temperature reached 400 °C, Oxygen gas given into the chamber and pressure increased to 300 Torr. Samples annealed in-situ at these conditions for an hour. After annealing, substrate temperature reduced to 200 °C with 10 °C/min ramp rate and then natural cooling took over. After temperature reached to 90 °C, chamber opened to atmosphere and then the samples removed from the chamber.

Crystal structure of the thin films determined by a PANalytical Empyrean X-Ray Diffractometer (XRD). Morphological structures and elemental analysis conducted with a Zeiss Sigma-300 Scanning Electron Microscope (SEM) - Energy Dispersive Spectroscopy (EDS) system.

3. Results

Thickness of the thin films are very small compared to substrate thickness. For this reason, we used "Grazing Incidence" XRD method (GIXRD) in order to avoid peaks from the substrates in thin films. YBCO is an air sensitive material and exposure to the air causes reflectivity profile to change (Han *et al.* 2003). GIXRD measurements for all thin films conducted with a grazing incidence angle of 0.5°. XRD peaks belonging to *c* oriented (*00l*) YBCO peaks (Zhai *et al.* 2001) and

XRD patterns of YBCO grown onto different substrates at the same conditions are given in Figure.1.

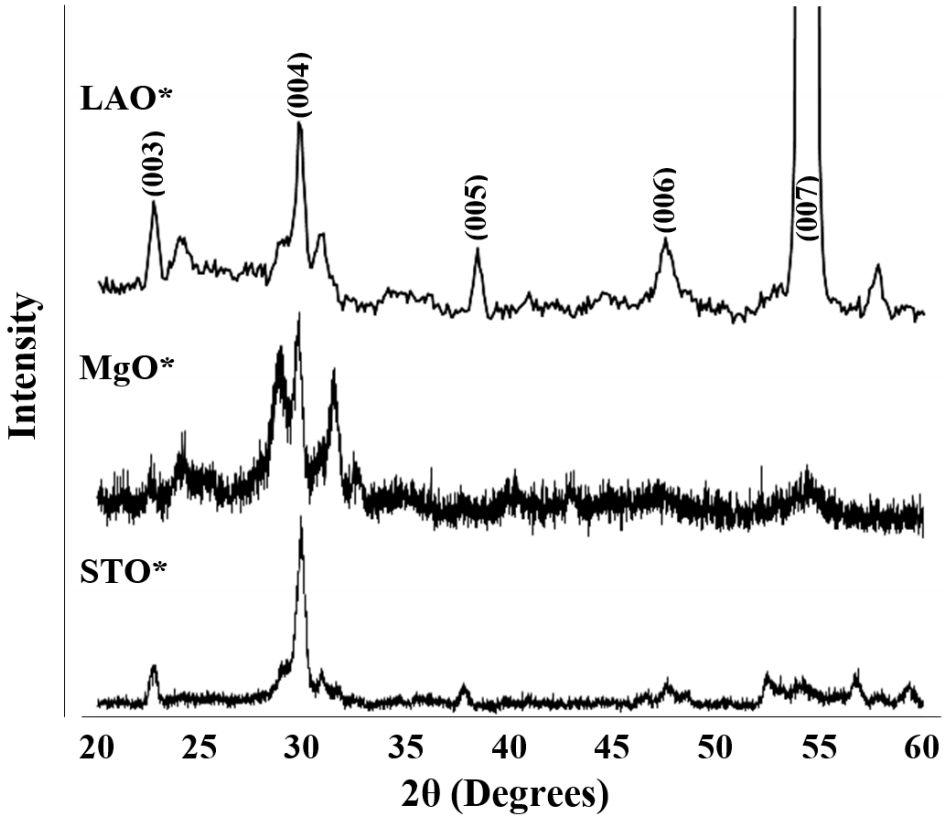

Figure.1. XRD patterns of YBCO grown onto different substrates.

It is clear from Figure.1 that YBCO thin film grown onto MgO substrate have random orientation compared to other substrates. Thin film over STO substrate is highly *c* oriented with maximum peak intensity in *(004)* direction. YBCO thin film grown onto LAO substrate have significantly high intensity in *(007)* direction with all *(00l)* directions present between 20 to 60 degrees (2θ) range. This result makes YBCO/LAO thin film top crystallinity over the other studied samples.

Surface morphologies of YBCO thin films analyzed with a SEM device and surfaces of different substrates are given with 1000 and 20000 times magnifications, in Figure.2, respectively.

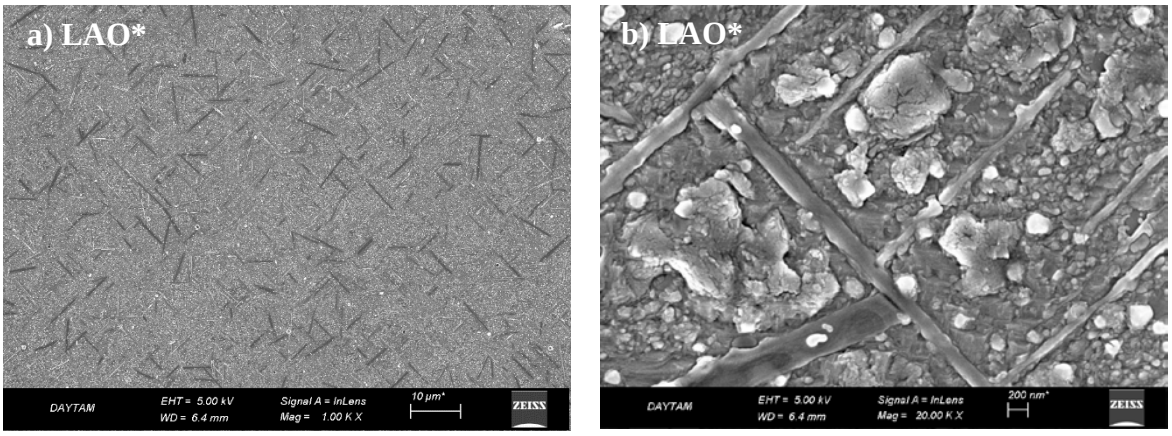

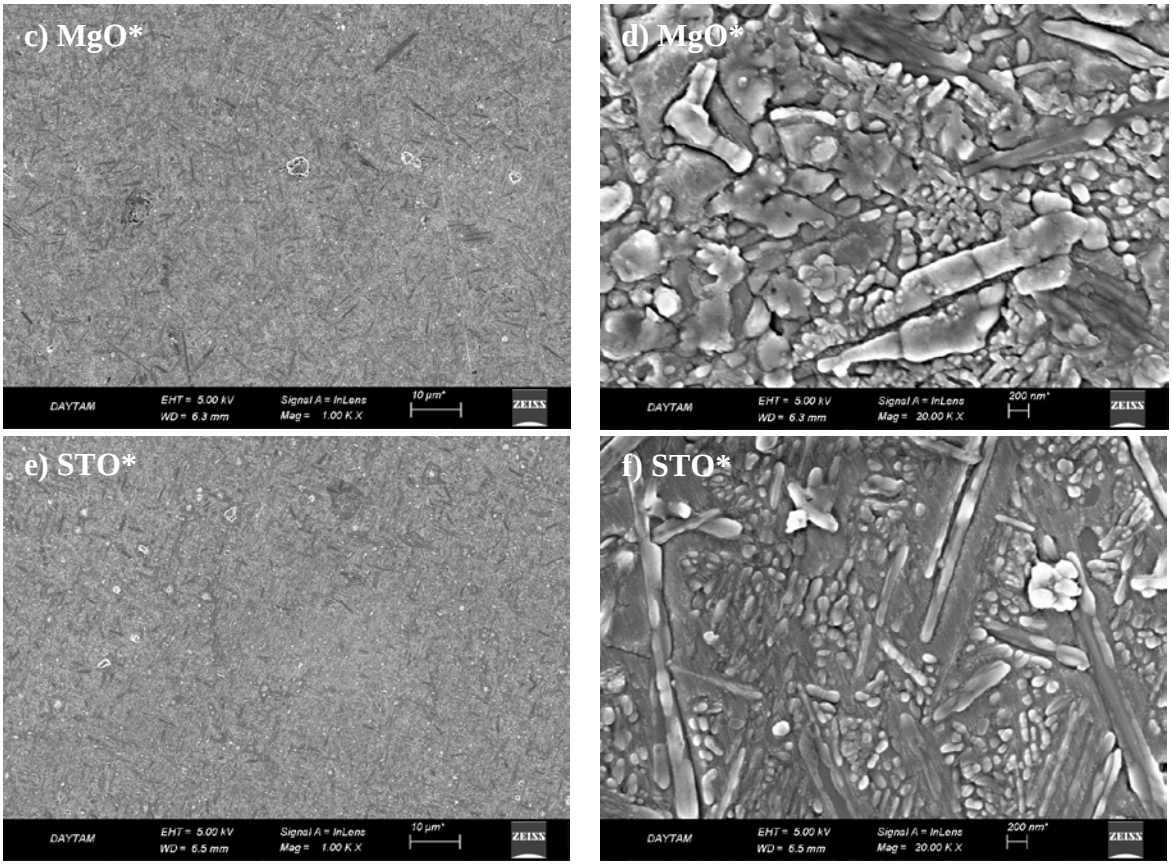

Figure.2. SEM images of YBCO thin films on different substrates **a)** LAO* (1000x), **b)** LAO* (20000x), **c)** MgO* (1000x), **d)** MgO* (20000x), **e)** STO* (1000x) and **f)** STO* (20000x)

Comparison of YBCO thin film surfaces with 1000 times magnification show that smallest droplet size and count caused by PLD techniques nature, observed in LAO compared to other substrates. All YBCO thin films on different substrates have rods parallel to the surfaces. Length of the rods in LAO substrate vary between 5-10 µm (Figure 2.a) with 100-300 nm thickness (Figure 2.b). Rods are shorter and random in MgO substrate; also, there are holes and more droplets over the surface (Figure.2.c). Thickness of each rod on MgO vary in its own compared to other substrates (Figure.2.d). There are more and bigger droplets over STO compared to LAO substrate with the length of 2-4 µm rods (Figure.2.e). Those rods over STO substrates have 100-250 nm thickness (Figure.2.f). SEM images reveal that none of the thin films has cracks caused by thermal expansion coefficient difference between substrate and YBCO thin films.

Elemental information of thin films on different substrates analyzed by EDS of the SEM system. All substrate and thin film elements present in analysis results (Figure.3) and their weight and atomic percent ratios shown in Table.2.

Table.2. Weight and atomic percent ratios of the thin films.

LAO*			MgO*			STO*		
Element	**Weight %**	**Atomic %**	**Element**	**Weight %**	**Atomic %**	**Element**	**Weight %**	**Atomic %**
O K	17.9	53.2	O K	27.9	42.5	O K	29.7	64.7
Al K	10.5	18.5	Mg K	51.9	52.1	Sr L	32.3	12.9
Y L	4.2	2.2	Y L	4	1.1	Y L	4	1.6
Ba L	8.8	3	Ba L	9.2	1.6	Ba L	6.6	1.7
La L	51.4	17.6	Cu K	7	2.7	Ti K	22.5	16.4
Cu K	7.3	5.5				Cu K	4.9	2.7

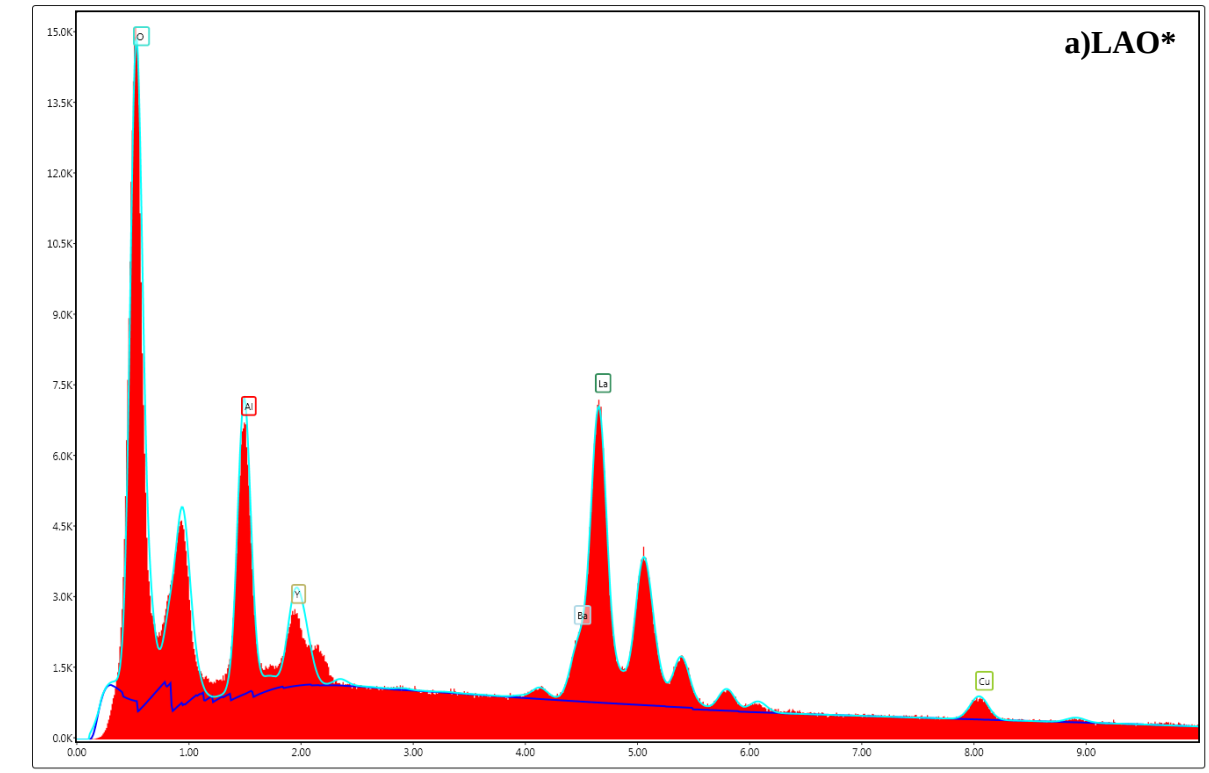
a)LAO*
O
Al
Y
La
Ba
Cu
15.0K
13.5K
12.0K
10.5K
9.0K
7.5K
6.0K
4.5K
3.0K
1.5K
0.0K
0.00
1.00
2.00
3.00
4.00
5.00
6.00
7.00
8.00
9.00
Status: Idle CPS: 29567 DT: 2.0 Lsec: 48.9 3.563K Cnts 5.090 keV Det: Element-C2

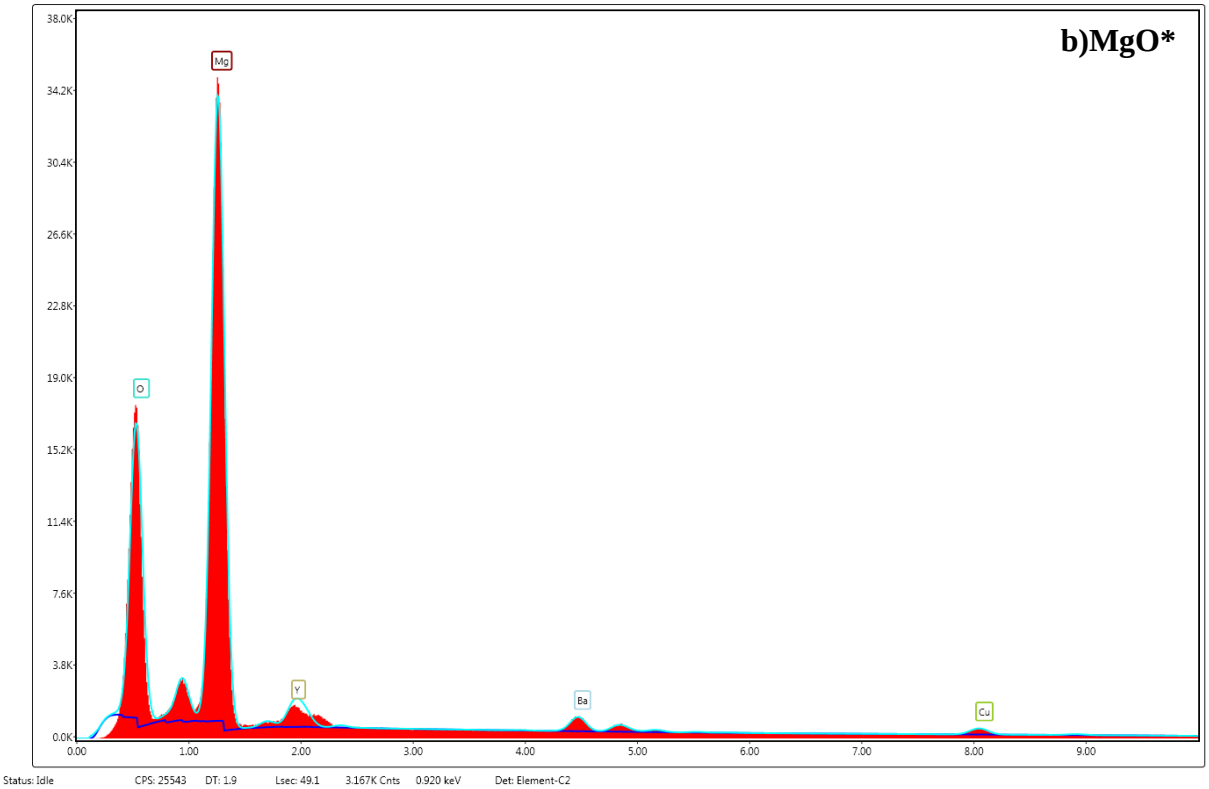
b)MgO*
Mg
O
Y
Ba
Cu
38.0K
34.2K
30.4K
26.6K
22.8K
19.0K
15.2K
11.4K
7.6K
3.8K
0.0K
0.00
1.00
2.00
3.00
4.00
5.00
6.00
7.00
8.00
9.00
Status: Idle CPS: 25543 DT: 1.9 Lsec: 49.1 3.167K Cnts 0.920 keV Det: Element-C2

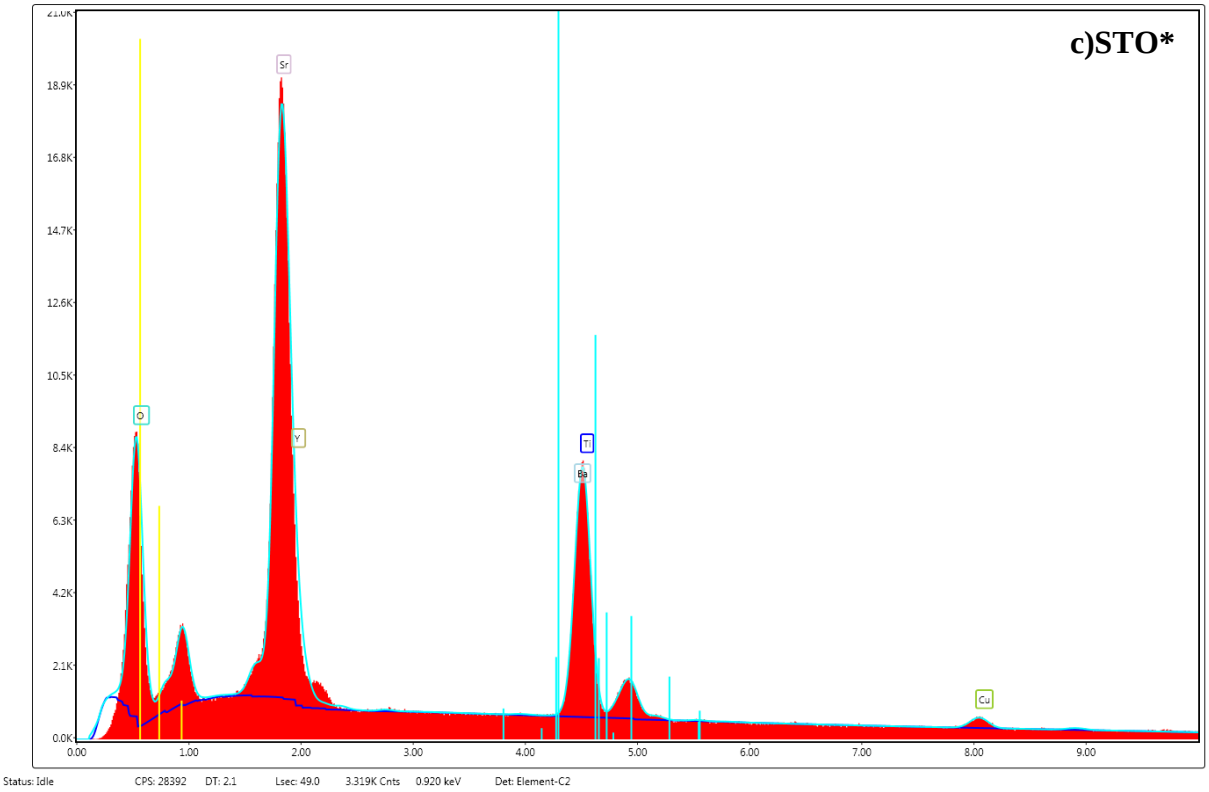

Figure.3. EDS analysis of thin films on **a)** LAO, **b)** MgO and **c)** STO substrates.

EDS analysis show that, YBCO thin film on LAO substrate have maximum Y, Ba and Cu atomic percent ratios. This result followed by STO substrate and MgO substrate has the lowest atomic percent for YBCO.

Thin film thickness measured with a KLA Tencor P-7 Stylus Profiler. Measured thickness was between 234-286 nm with an average of 260 nm. This result shows that approximately 0.43 Å / pulse achieved by PLD method with these fixed conditions.

As a result, YBCO thin films on LAO and STO substrates grown more successfully than MgO substrate. Lattice mismatch between YBCO and MgO single crystal are +10% in *a*-direction and +8% in *b*-direction, respectively. This result shows that lattice mismatch is very significant in thin film growth via PLD technique.

4. Conclusions

We have grown YBCO thin films on LAO, MgO and STO substrates at the same conditions by PLD technique and samples were in-situ annealed. XRD patterns of YBCO thin films revealed that thin film grown on MgO does not have any certain orientations. On the other hand, YBCO thin films grown on LAO and STO have high *c* orientations with very high intensity in LAO's *(007)* and high intensity in STO's *(004)* peaks. Comparison of SEM images of the YBCO thin films showed that thin film grown on LAO has the least and smallest droplets on the surface. All three thin film surfaces have rods with different sizes parallel to the surface. EDS analysis showed that Y, B and Cu elements are least found in thin film grown on MgO substrate. Compared to each other, LAO substrate has the best and MgO substrate has the worse thin film growth.

This study shows that substrate materials' lattice parameters affect the thin film properties significantly in PLD technique. MgO is a very sensitive material to moisture and if it is required as a substrate material for YBCO thin film growth, a suitable buffer layer is highly recommended between YBCO and MgO substrate. We strongly recommend LAO as YBCO thin film substrate for its close lattice match to YBCO. In addition, it is shown that, STO is a good substrate candidate for YBCO thin films, in case a substrate with a higher dielectric constant is required for device applications.

References

ABOUDIHAB, I., GILABERT, A., AZEMA, A. and ROUSTAN, J.C., 1994. Superconducting $YBa_2Cu_3O_{7-X}$ thin film

bolometer for infrared radiation. Superconductor Science & Technology, 7 (2), 80-83.

BIERLEUTGEB, K. and PROYER, S., 1997. Pulsed-laser deposition of Y-Ba-Cu-O films: the influence of fluence and oxygen pressure. Applied Surface Science, 109-110, 331-334.

CHRISEY, D.B. and HUBLER, G.K., 1994. Pulsed Laser Deposition of Thin Films. Wiley-Interscience, 613 p, New York.

DUHALDE, S., LAMAGNA, A., VILLAFUERTE, M., SCHWARTZMAN, A., CORRERA, L. and QUINTANA, G., 1998. Influence of the deposition parameters on the structural and transport properties of YBaCuO thin films prepared by pulsed laser deposition. Applied Surface Science, 127, 520-524.

HAN, S.-W., TRIPATHY, S., MICELI, P., BADICA, E., COVINGTON, M., GREENE, L. and APRILI, M., 2003. X-ray reflectivity study of interdiffusion at YBa2Cu3O7-x and metal interfaces. Japanese Journal of Applied Physics, 42 (3R), 1395.

KAWASHIMA, J., YAMADA, Y. and HIRABAYASHI, I., 1998. Critical thickness and effective thermal expansion coefficient of YBCO crystalline film. Physica C: Superconductivity, 306 (1-2), 114-118.

KIM, S.M. and LEE, S.Y., 1999. Characterization of YBCO superconducting films fabricated by pulsed laser deposition. THIN SOLID FILMS, 355, 461-464.

LEE, L.P., LONGO, J., VINETSKIY, V. and CANTOR, R., 1995. Low-noise $YBa_2Cu_3O_{7-\delta}$ direct-current superconducting quantum interference device magnetometer with direct signal injection. Applied Physics Letters, 66 (12), 1539-1539.

LEE, S.Y., JIA, Q.X., ANDERSON, W.A. and SHAW, D.T., 1991. In situ laser deposition of superconducting $YBa_2Cu_3O_{7-x}$ thin films on GaAs substrates. Journal of Applied Physics, 70 (11), 7170-7170.

LI, C., WANG, X., WANG, J., SUN, L. and HE, Y., 2017. Progress on applications of high temperature superconducting microwave filters. Superconductor Science and Technology, 30 (7), 073001.

PHILLIPS, J.M., 1996. Substrate selection for high-temperature superconducting thin films. Journal of Applied Physics, 79 (4), 1829-1848.

PROYER, S. and STANGL, E., 1995. Time-Integrated Photography of Laser-Induced Plasma Plumes. Applied Physics A-Materials Science & Processing, 60 (6), 573-580.

PROYER, S., STANGL, E., BORZ, M., HELLEBRAND, B. and BAUERLE, D., 1996. Particulates on Pulsed-Laser Deposited Y-Ba-Cu-O films. Physica C, 257 (1-2), 1-15.

WU, M.K., ASHBURN, J.R., TORNG, C.J., HOR, P.H., MENG, R.L., GAO, L., HUANG, Z.J., WANG, Y.Q. and CHU, C.W., 1987. Superconductivity at 93 K in a new mixed-phase Yb-Ba-Cu-O compound system at ambient pressure. Physical Review Letters, 58 (9), 908-910.

YANMAZ, E., BASOGLU, M. and GROVENOR, C.R.M., 2009. Anomalous ferromagnetic behaviour of Y_2O_3 and CuO nanoparticles in $YBa_2Cu_3O_y$ superconductor. Physica Status Solidi A-Applications and Materials Science, 206 (12), 2844-2850.

YURTCAN, M.T., 2011. YBCO İnce Filmlerin Darbeli Lazer Yığma Tekniğiyle Hazırlanması. PhD Thesis, Atatürk University, Erzurum.

YURTCAN, M.T., SIMSEK, O., YILMAZ, M., HASAR, U.C., ERTUGRUL, M. and BAYRAM, O.S., 2013. Influence of Deposition Pressure (O_2) on the YBCO (Y123) Thin Films Prepared by Pulsed Laser Deposition. Journal of Superconductivity and Novel Magnetism, 26 (5), 1873-1877.

ZHAI, H.Y., ZHANG, Z.H. and CHU, W.K., 2001. Accurate comparative measurement of oxygen content variations in YBa2Cu3O7−δ films due to postdeposition annealing. Applied Physics Letters, 78 (5), 649-651.

Phenomenological and Microscopic Analysis of Elastic Scattering Reactions of ^{20}Ne by ^{12}C, ^{16}O, ^{28}Si, ^{58}Ni

MURAT AYGÜN

Department of Physics, Bitlis Eren University, Bitlis 13000, Turkey

Abstract

In this study, the elastic scattering angular distributions of ^{20}Ne from ^{12}C, ^{16}O, ^{28}Si and ^{58}Ni target nuclei have been investigated at various incident energies. For this, both the phenomenological model and the double folding model have been used. In the phenomenological calculations, the real and imaginary potentials have been evaluated in Woods-Saxon type. In the double folding calculations, the imaginary part has been assumed as Woods-Saxon potential while the real part has been obtained by using the folding model. The theoretical results have been compared with the literature as well as the experimental data. It has been observed that our results have been in agreement with the experimental data. Also, the cross-sections of the investigated system and models have been given.

Keywords: Optical model, double folding model, elastic scattering.

1. Introduction

The optical model (OM) is one of the most effective methods in explaining the elastic scattering cross section of projectile by target nucleus. To determine the optical potential of system investigated, the phenomenological model (PM) and the double folding model (DFM) (SATCHLER and Love, 1979) are often applied. Thus, the optical potential is obtained by searching of the potential parameters of model assumed. It is well-known that the OM parameters are extensively used in the calculations of elastic scattering, coupled-channels, transfer reactions. While the OM parameters for multiple systems are defined, one of the most preferred ways is to find the parameters for the same potential geometry of the systems.

Received: 22.05.2017
Revised: 07.08.2017
Accepted:28.09.2017
Corresponding author: Murat Aygun, PhD
Department of Physics, Bitlis Eren University, Bitlis 13000, Turkey
E-mail: murata.25@gmail.com
Cite this article as: M. Aygun, Phenomenological and Microscopic Analysis of Elastic Scattering Reactions of ^{20}Ne by ^{12}C, ^{16}O, ^{28}Si, ^{58}Ni, Eastern Anatolian Journal of Science, Vol. 3, Issue 2, 8-15, 2017.

Due to the fact that the interactions of projectile with different target nuclei have different potentials, it is difficult to work on the same potential geometry. Consequently, establishing potential parameters has been both difficult and important in the examination of nuclear reactions. In literature, the theoretical studies performed with this goal can be found at Ref. (AYGUN, 2014; AYGUN et al. 2010).

In the last few decades, various experimental and theoretical studies have been carried out on ^{20}Ne nucleus (PIASECKI et al. 2012; PARKER et al. 1987; TILLEY, 1998; SINGH et al. 2008; HEIL et al. 2014). Some of these works have been on the elastic scattering of ^{20}Ne nucleus with different target nuclei over several incident energies. Doubre et al. (1978) measured the elastic scattering of ^{20}Ne+^{12}C system at E_{Lab}=65.86 MeV and analyzed the experimental data by means of the OM. Bohlen et al. (1993) reported the elastic scattering, inelastic scattering and one neutron transfer channels of ^{20}Ne+^{12}C system at E_{Lab}=390 MeV. They performed the OM and DFM analysis to explain the experimental data of this system which presents a strong absorption. Miao et al. (1996) obtained the elastic scattering angular distributions of ^{20}Ne+^{16}O system at different energies. To explain the experimental data, they presented the theoretical results acquired by using the OM. The elastic scattering data of ^{20}Ne on ^{28}Si have been reported by (SOUKERAS, 2013; SGOUROS, 2013; SGOUROS et al. 2013). They analyzed the experimental data with the distorted wave born approximation (DWBA), the OM and the coupled reaction channels (CRC). Bohlen et al. [1985] measured the elastic scattering of ^{20}Ne+^{58}Ni system at E_{Lab}=291 and 392 MeV and investigated the experimental data within the OM. However, as far as we know, if one seeks the optical potential parameters for the same potential geometry of these systems, one can not find them in literature. We aim to obtain the potential parameters of ^{20}Ne+^{12}C, ^{20}Ne+^{16}O, ^{20}Ne+^{28}Si and ^{20}Ne+^{58}Ni reactions at different incident energies with the same potential geometry. Thus, these potential parameters will be able to use in the calculations of both new energies of these systems with ^{20}Ne and different nucleus reactions with ^{20}Ne. Additionally, these parameters will be important in the experimental analysis of

coupled-channels, transfer reactions, α-folding model of ^{20}Ne.

In this study, we examine ^{20}Ne-nucleus reactions with a phenomenological way within the framework of OM. Then, we analyze all the reactions by using the DFM within the microscopic model. We show the optical potential parameters of the PM and DFM. Finally, we compare the PM and DFM results with previous theoretical and experimental studies.

2. Theoretical Formalism

In the present work, the elastic scattering data of ^{20}Ne is investigated using PM and DFM at various incident energies. For this, different target nuclei are used from ^{12}C to ^{58}Ni. In this concept, the total effective potential, $V_{total}(r)$, is given by,

$$V_{total}(r) = V_{nuclear}(r) + V_{Coulomb}(r) \quad (1)$$

where $V_{nuclear}(r)$ is nuclear potential and $V_{Coulomb}(r)$ is Coulomb potential. The Coulomb potential is taken as (SATCHLER, 1983),

$$V_{Coulomb}(r) = \begin{cases} \frac{1}{4\pi\varepsilon_0}\frac{Z_P Z_T e^2}{r}, & r \geq R_C \\ \frac{1}{4\pi\varepsilon_0}\frac{Z_P Z_T e^2}{2R_C}\left(3 - \frac{r^2}{R_C^2}\right), & r < R_C \end{cases} \quad (2)$$

$$R_c = 1.25\left(A_P^{1/3} + A_T^{1/3}\right) \quad (3)$$

where Z_P and Z_T, respectively, are the charges of the projectile and target nuclei, R_c is the Coulomb Radius, A_P and A_T are the projectile and target masses, respectively.

2.1 Phenomenological Model Analysis

In general sense, the PM assumes Woods-Saxon (WS) or Woods-Saxon squared (WS^2) type potentials for the real and imaginary parts of the optical potential. In this sense, the nuclear potential is given by,

$$V_{nuclear}(r) = -\frac{V_0}{1+\exp\left(\frac{r-r_v\left(A_P^{1/3}+A_T^{1/3}\right)}{a_v}\right)} - \frac{iW_0}{1+\exp\left(\frac{r-r_w\left(A_P^{1/3}+A_T^{1/3}\right)}{a_w}\right)} \quad (4)$$

The potential parameters are obtained by searching of the values which fit the experimental data. This procedure is described below.

2.2 Double Folding Model Analysis

The DFM gives the real part of the optical potential over the densities of projectile and target nuclei by using an nucleon-nucleon interaction potential (v_{NN}). For this purpose, the double folding potential is written as,

$$V_{\mathrm{DF}}(\boldsymbol{r}) = \int d\boldsymbol{r_1} \int d\boldsymbol{r_2} \rho_P(\boldsymbol{r_1}) \rho_T(\boldsymbol{r_2})\, v_{NN}(r_{12}) \quad (5)$$

where $\rho_P(\boldsymbol{r_1})$ and $\rho_T(\boldsymbol{r_2})$ are the nuclear matter densities of projectile and target nuclei, respectively. In the present work, the density distributions of both projectile and target nuclei except for ^{12}C have been taken from RIPL-3 (RIPL-3). ^{12}C density is written as,

$$\rho_{12_C}(r) = \rho_0(1 + wr^2)\exp(-\beta r^2) \quad (6)$$

where ρ_0 = 0.1644 fm^{-3}, w = 0.4988 fm^{-2}, and β = 0.3741 fm^{-2} (FARID and HASSANIAN, 2000; KARAKOC and BOZTOSUN, 2006). In Fig. 1, the proton and neutron density distributions used for ^{20}Ne nucleus are displayed. In folding model calculations, we have chosen the M3Y (Michigan 3 Yukawa) nucleon-nucleon realistic interaction given by,

$$v_{NN}(r) = 7999\frac{\exp(-4r)}{4r} - 2134\frac{\exp(-2.5r)}{2.5r} - 276[1 - 0.005E_{\mathrm{Lab}}/A_P]\delta(r) \quad (7)$$

Finally, the imaginary part of optical potential is assumed WS type as in the form

$$W(r) = -\frac{W_0}{1+\exp\left(\frac{r-r_w\left(A_P^{1/3}+A_T^{1/3}\right)}{a_w}\right)} \quad (8)$$

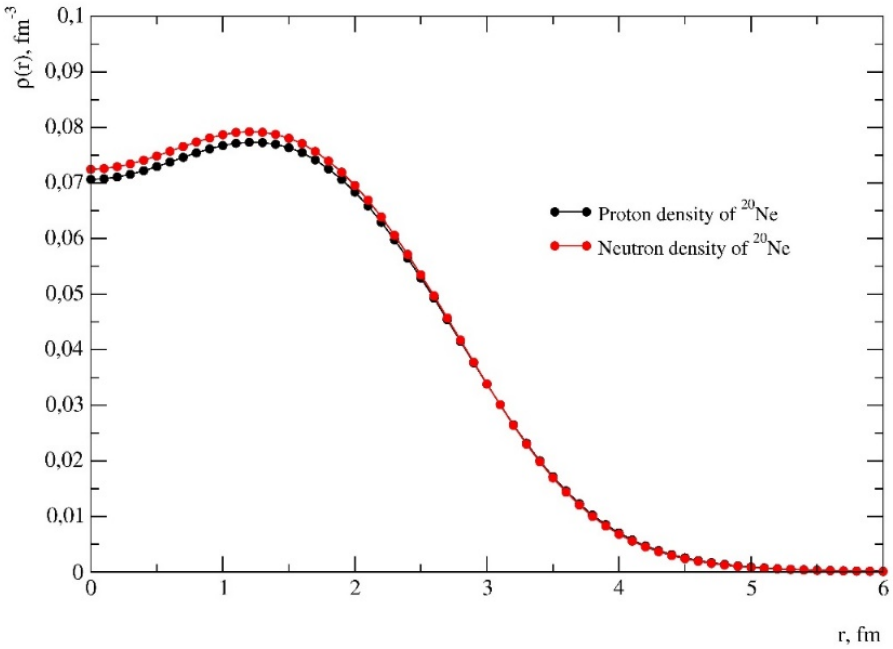

Figure 1. The proton and neutron density distributions of ^{20}Ne nucleus.

2.3 Fitting Procedure

In this section, we introduce fitting procedure used in PM and DFM calculations. While the values of the real and imaginary potentials to be used in the phenomenological analysis have been defined, we have started from the potential values reported in the literature (DOUBRE et al. 1978; BOHLEN et al. 1993; MIAO et al. 1996; SOUKERAS, 2013; BOHLEN et al. 1985). Then, we have performed compliance tests between the experimental data and the theoretical results of all the systems investigated in our work. In order to obtain the OM parameters at the same potential geometries of reactions, we have searched the values of r_v=r_w and a_v=a_w. After the test calculations performed to obtain results compatible with the experimental data, we have taken as 0.913 fm the values of r_v=r_w. Then, for this value of r_v and r_w, we have examined the values of a_v and a_w which give good agreement results with the data. We have found 0.78 fm for a_v = a_w. We have eventually searched V_0 and W_0 values at the values determined of r_v=r_w and a_v=a_w. We have given the OM parameters obtained for all the reactions by means of the PM in Table I.

In DFM calculations, the values W_0, r_w and a_w of imaginary potential have been obtained as described above. According to this, firstly, the value r_w in steps of 0.1 fm at each incident energy has been investigated and kept constant at 1.32 fm. Then, the value a_w of imaginary potential has been varied in steps of 0.1 and 0.01 fm for fixed radius and has been taken as 0.55 fm. Finally, the fitting procedure has been completed by adjusting only the depth of imaginary potential. The optical potential parameters of all the reactions within the framework of DFM have been shown in Table II.

The code FRESCO (THOMPSON, 1988) has been used in the theoretical calculations.

3. Results and Discussion

We have analyzed the elastic scattering data of ^{20}Ne+^{12}C reaction at incident energies E_{Lab}=65.86 and 390 MeV. For this, we have used the PM and the DFM within the framework of OM. The values of potential parameters for each model are given in Tables I and II. Also, all theoretical results with PM and DFM are compared with the experimental data as shown in Fig. 2. Although it is difficult to define the potential parameters because of both the oscillatory structure of experimental data and the same potential geometry of the systems, the results are in agreement with the experimental data for the PM and the DFM at 65.86 MeV. At 390 MeV, we have obtained very good results with the data at all angles for the PM, whereas the DFM results are not as good as the PM results. We have found a deep imaginary potential which means a strong absorption in the analysis of PM. This result is similar to the result of Ref. (BOHLEN et al. 1993). In folding model calculations, we have also investigated the change of normalization constant (N_R) and have given N_R values for examined system and energy in Table II.

Table I. The OM parameters used in PM analysis of ^{20}Ne scattered from ^{12}C, ^{16}O, ^{28}Si and ^{58}Ni target nuclei.

System	E_{Lab}	V	r_v	a_v	W	r_w	a_w	σ
	MeV	*MeV*	*fm*	*fm*	*MeV*	*fm*	*fm*	*mb*
^{20}Ne+^{12}C	65.86	24.3	0.913	0.78	5.70	0.913	0.78	736.6
	390	75.0	0.913	0.78	88.0	0.913	0.78	1742.8
^{20}Ne+^{16}O	45	49.4	0.913	0.78	2.42	0.913	0.78	475.2
	53.75	84.0	0.913	0.78	5.10	0.913	0.78	808.6
^{20}Ne+^{28}Si	42.5	148	0.913	0.78	26.0	0.913	0.78	393.8
	52.3	109	0.913	0.78	27.0	0.913	0.78	704.4
^{20}Ne+^{58}Ni	291	128	0.913	0.78	36.0	0.913	0.78	1911.0
	392	142	0.913	0.78	71.0	0.913	0.78	2214.4

Table II. The OM parameters used in DFM analysis of ^{20}Ne scattered from ^{12}C, ^{16}O, ^{28}Si and ^{58}Ni target nuclei.

System	E_{Lab}	N_R	W	r_w	a_w	σ
	MeV		*MeV*	*fm*	*fm*	*mb*
^{20}Ne+^{12}C	65.86	0.407	4.60	1.32	0.55	1071.5
	390	0.749	22.0	1.32	0.55	1826.1
^{20}Ne+^{16}O	45	0.60	4.10	1.32	0.55	754.2
	53.75	0.80	5.95	1.32	0.55	1034.5
^{20}Ne+^{28}Si	42.5	1.00	8.0	1.32	0.55	464.5
	52.3	1.00	22.0	1.32	0.55	991.4
^{20}Ne+^{58}Ni	291	0.78	9.30	1.32	0.55	2377.8
	392	0.93	10.5	1.32	0.55	2499.5

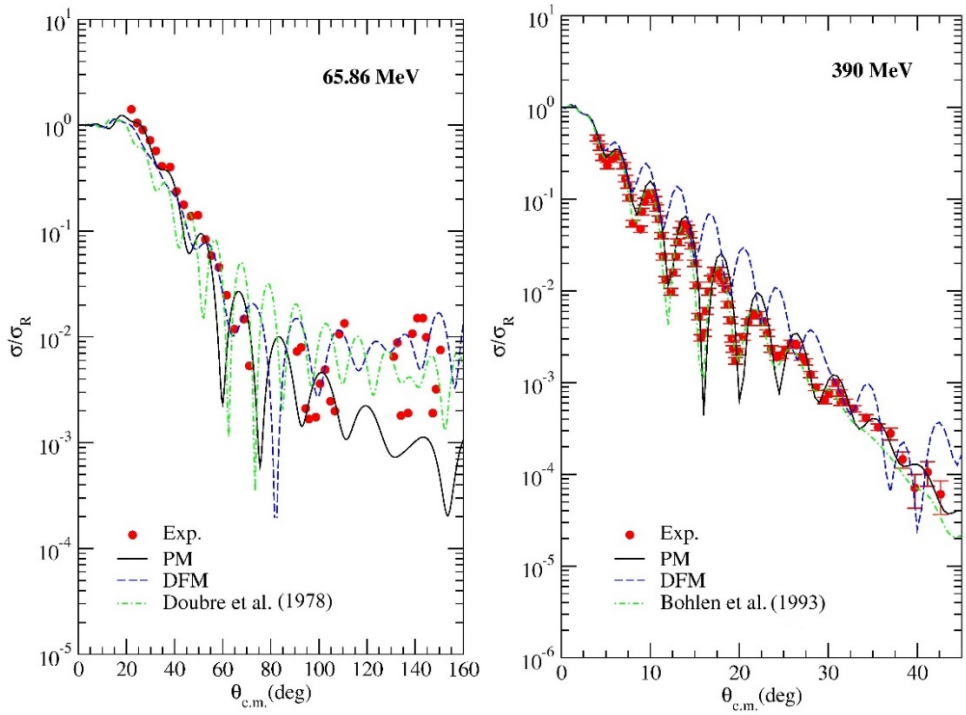

Figure 2. The elastic scattering angular distributions for ^{20}Ne+^{12}C at E_{Lab}=65.86 and 390 MeV. The solid lines show PM results; dashed lines show DFM results and dot-dashed lines show the results obtained by Doubre et al. (1978) and Bohlen et al. (1993). The circles show the experimental data, which have been taken from (DOUBRE et al. 1978; BOHLEN et al. 1993).

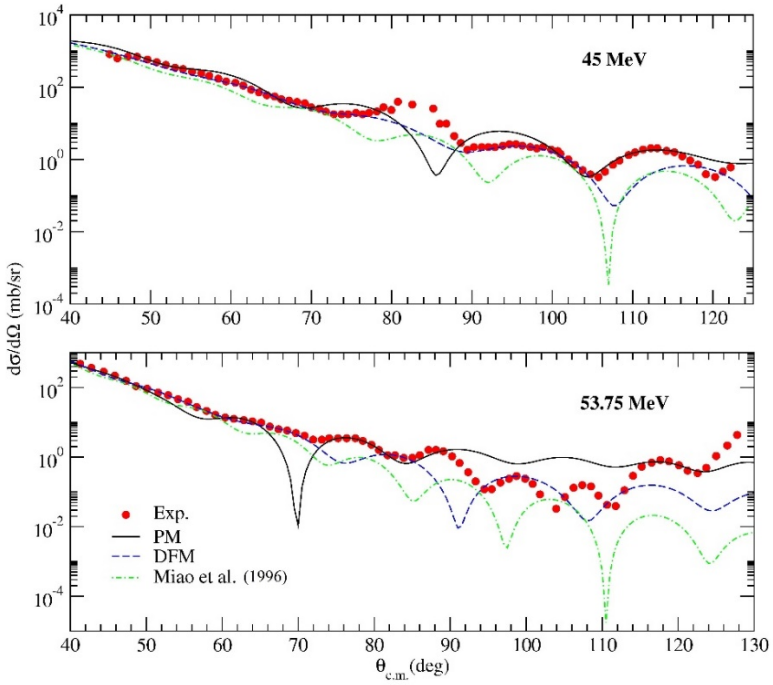

Figure 3. The elastic scattering angular distributions for ^{20}Ne+^{16}O at E_{Lab}=45 and 53.75 MeV. The solid lines show PM results; dashed lines show DFM results and dot-dashed lines show the results obtained by Miao et al. (1996). The circles show the experimental data, which have been taken from (MIAO et al. 1996).

^{20}Ne+^{16}O which has the elastic scattering data at E_{Lab}=45 and 53.75 MeV is another system investigated in our study. ^{20}Ne+^{16}O has an oscillation data for these energies. We have given the values of potential parameters obtained from the theoretical calculations of each model in Tables I and II. In Fig. 3, the theoretical results of the PM and the DFM have been exhibited in comparison with the results of the literature (MIAO et al. 1996). We have observed that the PM results are in good agreement with data and are also better than the results of Ref. (MIAO et al. 1996). In addition to this, the results of DFM are better than the the results of Ref. (MIAO et al. 1996).

In our work, we have also studied the elastic scattering of ^{20}Ne by ^{28}Si at E_{Lab}=42.5 and 52.3 MeV. Theoretical results obtained for the values shown in Tables I and II have given a satisfactory description for the experimental data, which are plotted in Fig. 4. Especially, this case is very clear at 42.5 MeV. The DFM results are in very good agreement with the data. A deep imaginary potential has been used in the calculations of PM (at all energies) and DFM (especially at 52.3 MeV) in order to obtain the general slope of the experimental data.

In final analysis, we have investigated the elastic scattering angular distribution of ^{20}Ne+^{58}Ni system at E_{Lab}=291 and 392 MeV. In Fig. 5, we have exhibited all theoretical results as comparative with the previous study (BOHLEN et al. 1985) as well as the experimental data. The consistence between PM and DFM according to the experimental data is quite good. Then, we have compared our results with the results of the literature and have noticed that both PM and DFM results are good as that of the results of Ref. (BOHLEN et al. 1985).

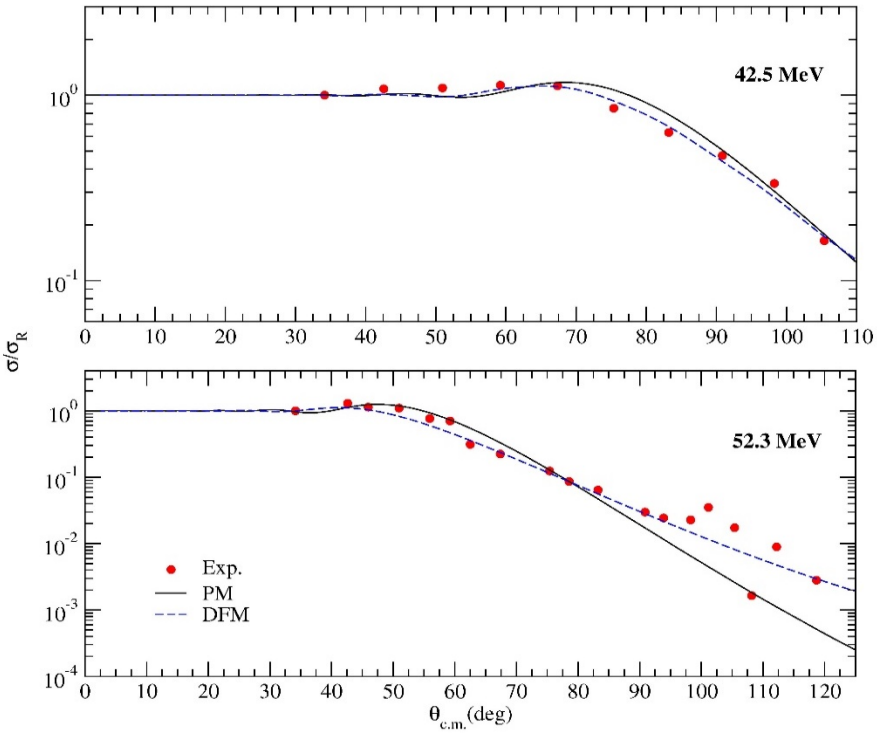

Figure 4. The elastic scattering angular distributions for ^{20}Ne+^{28}Si at E_{Lab}=42.5 and 52.3 MeV. The solid lines show PM results; dashed lines show DFM results. The circles show the experimental data, which have been taken from (SOUKERAS, 2013).

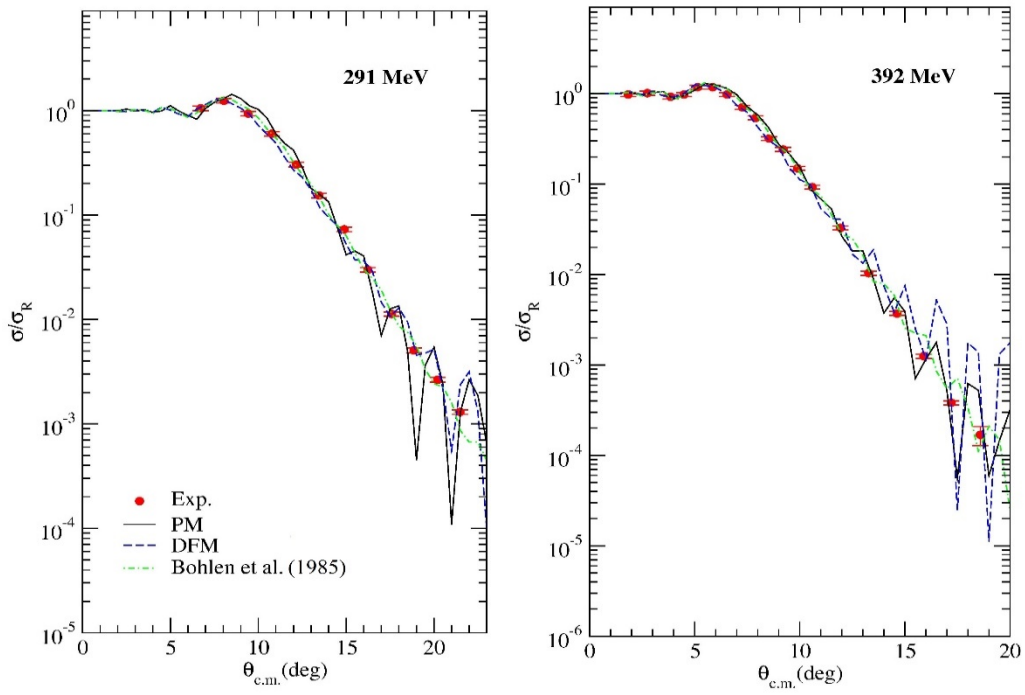

Figure 5. The elastic scattering angular distributions for ^{20}Ne+^{58}Ni at E_{Lab}=291 and 392 MeV. The solid lines show PM results; dashed lines show DFM results and dot-dashed lines show the results obtained by Bohlen et al (1985). The circles show the experimental data, which have been taken from (BOHLEN et al. 1985).

In Tables I and II, we have shown the cross-section (σ) values for all the systems investigated.
We have observed that the theoretical cross-sections of all interactions from ^{12}C to ^{58}Ni present similar behaviors with increasing of the energy. As known from previous study (AYGUN, 2012), it can be said that similar cross-sections obtained for different OM calculations such as the PM and the DFM denote good fits of the elastic scattering angular distributions.

4. Conclusions

In the present work, the elastic scattering angular distributions of ^{20}Ne on ^{12}C, ^{16}O, ^{28}Si and ^{58}Ni target nuclei have been examined. In this context, both the PM and the DFM analysis have been performed in order to explain the experimental data. The theoretical results have been compared with the results of previous studies and the experimental data. It has been noticed that our results are in agreement both with the each other and the data. The potential parameters for both investigated systems and energies by using these methods have been determined and given in tables. It can be said that the application of potential parameters obtained for ^{20}Ne interactions using the PM and the DFM based on the OM will be reliable and practical in the calculations of elastic scattering, coupled-channels, transfer reactions, α-folding model etc., of unknown reaction and energies. Moreover, the cross-sections of all the reactions have been provided. Similar behaviors of cross-sections obtained by using different OM approaches such as the PM and the DFM can be attributed to good fits of the elastic scattering angular distributions.

References

SATCHLER, G.R. and LOVE, W.G., (1979), *Folding model potentials from realistic interactions for heavy-ion scattering*, Physics Report, 55, 3.

AYGUN, M., (2014), *A microscopic analysis of elastic scattering of ^{8}Li nucleus on different target nuclei*, Acta Phys. Pol. B, 45, 9.

AYGUN, M., KUCUK, Y., BOZTOSUN, I. and IBRAHEEM, A.A., (2010), *Microscopic few-body and gaussian-shaped density distributions for the analysis of the ^{6}He exotic nucleus with different target nuclei*, Nuclear Physics A, 848, 245-259.

PIASECKI, E., et al., (2012), *Weak channels in backscattering of ^{20}Ne on ^{nat}Ni, ^{118}Sn, and ^{208}Pb*, Physical Review C, 85, 054604.

PARKER, D.J., HOGAN, J.J. and ASHER, J., (1987), *Complete and incomplete fusion in ^{20}Ne + ^{58}Nb reactions*, Physical Review C, 35, 1.

TILLEY, D.R., CHEVES, C.M., KELLEY, J.H., RAMAN, S. and WELLER, H.R., (1998), *Energy levels of light nuclei A = 20*, Nuclear Physics A, 636, 249-364.

SINGH, D., ALI R., AFZAL ANSARI, M., RASHID, M.H., GUIN, R. and DAS, S.K., (2009), *Reaction mechanisms in the system ^{20}Ne + ^{165}Ho: Measurement and analysis of forward recoil range distributions*, Physical Review C, 79, 054601.

HEIL, M., et al., (2014), *Stellar neutron capture cross sections of ^{20,21,22}Ne*, Physical Review C, 90, 045804.

DOUBRE, H., ROYNETTE, J.C., PLAGNOL, E., LOİSEAUX, J.M., MARTİN, P. and DE SAINTIGNON, P., (1978), *Experimental study of the ^{20}Ne+ ^{12}C system*, Physical Review C, 17, 131.

BOHLEN, H.G., et al., (1993), *Refractive scattering and reactions, comparison of two systems:^{16}O+^{16}O and ^{20}Ne+^{12}C*, Zeitschrift für Physik A Hadrons and Nuclei, 346, 189-200.

MIAO, Y., ZURMÜHLE R.W., BARROW, S.P., WIMER, N.G., MURGATROYD, J.T., LEE, C. and LIU, Z., (1996), *Resonant structures in the ^{20}Ne+^{16}O system*, Physical Review C, 53, 2.

SOUKERAS, V., (2013), *Elastic scattering for the system ^{20}Ne+^{28}Si at near barrier energies*, University of Ioannina, MSc Dissertation.

SGOUROS, O., (2013), *Transfer reactions for the system ^{20}Ne+^{28}Si at near barrier energies*, Master Thesis, University of Ioannina.

SGOUROS, O., et al., (2013), *Backward angle structure in the ^{20}Ne+^{28}Si quasielastic scattering*, International Journal of Modern Physics Letters E, 22, 10.

BOHLEN, H.G., OSSENBRINK, H., LETTAU, H. and OERTZEN, W.Y., (1985), *Inelastic scattering of ^{20}Ne and ^{12}C on ^{58}Ni and the three-body continuum*, Zeitschrift für Physik A Hadrons and Nuclei, 320, 237-251.

SATCHLER, G.R., (1983), *Direct Nuclear Reactions* (*Oxford University Press, Oxford*). Reference Input Parameter Library (RIPL-3), http://www-nds.iaea.org/RIPL-3.

EL-AZAB FARID, M. and HASSANIAN, M.A., (2000), *Density-independent folding analysis of the ^{6,7}Li elastic scattering at intermediate energies*, Nuclear Physics A, 678, 39.

KARAKOC, M. and BOZTOSUN, I., (2006), *α−α double folding cluster potential description of the ^{12}C+^{24}Mg system*, Physical Review C, 73, 047601.

THOMPSON, I.J., (1988), *Coupled reaction channels calculations in nuclear-physics*, Computer Physics Reports, 7, 167.

AYGUN, M., (2012), *Double-folding analysis of the ^{6}Li + ^{58}Ni reaction using the ab initio density distribution*, European Physial Journal A, 48, 145.

Performance Analysis of Speed Control of PMDC Motor using Fuzzy Logic Controller

MUHAMMED REŞİT ÇORAPSIZ[1]

[1]*Department of Electrical and Energy, Bayburt University, 69000, Bayburt, Turkey*

Abstract

In this study, performance analysis of speed control of PMDC (Permanent Magnet Direct Current) motor using fuzzy logic controller was realized in Matlab/SIMULINK environment. Firstly, the mathematical model was obtained using the mechanical and electrical values of electrical equivalent circuit of the DC motor. Then, the fuzzy logic and PI controller structures was designed. Different references speeds were applied to the systems controlled by the FL and the PI controller. Additionally, in this study, the effect of varying armature resistance of the PMDC motor on the controller structures used in simulations and on the speed of the PMDC motor was also investigated. Comparisons were made for both controllers considering the same conditions. According to the results obtained by using the data in this study, it is observed that the fuzzy logic controller has a better performance than the PI controller.

Key words: DC Motor Control, Fuzzy Logic Controller, Variable Armature Resistance, PI Controller, Matlab/SIMULINK

1. Introduction

The PMDC motor is an electric machine that converts direct current electrical energy into the mechanical energy. These machines basically consist of two main parts. The stator is fixed and the rotor rotates.

Received: 12.07.2017
Revised: 28.09.2017
Accepted: 03.10.2017
Corresponding author: Muhammed Reşit Çorapsız, Department of Electrical and Energy, Bayburt University, 69000, Bayburt, Turkey
E-mail: rcorapsiz@bayburt.edu.tr
Cite this article as: M. R. Çorapsız, Performance Analysis of Speed Control of PMDC Motor using Fuzzy Logic Controller, Eastern Anatolian Journal of Science, Vol. 3, Issue 2, 16-29, 2017.

Because of their high reliabilities, flexibilities and low costs, DC motors are widely used in industrial applications, robot manipulators and home appliances where speed and position control of motor are required (AHMED et al, 2013). Speed or position control in these machines is easier than other electric machines, so they were preferred in the industry (AÇIKGÖZ, ŞEKKELİ, 2013). DC motors are widely used in industrial control applications due to their simple structures and they have been the subject of many fields of research and development in the industrial control applications. However, they require maintenance because of contact of commutator and brushes with each other. DC motors are most suitable for wide range of speed control and there are many adjustable speed drives (BANSAL, NARVEY, 2013). Control of these motors has become necessary in applications that require a certain amount of power, movement, speed. Classic Control has proven, for a long time, to be good enough to handle control tasks on system control; however, its implementation relies on an exact mathematical model of the plant to be controlled but simple mathematical operations (SALIM et al., 2013).

In this study, firstly, PMDC motor model was designed in Matlab/SIMULINK environment and speed control was performed with fuzzy logic and PI controller. Then, the controllers were compared for different reference speed inputs. Finally, in order to investigate the effect of armature resistance change on the controller structures used in simulations, armature resistances were changed at certain values and the effects were observed. Thus, it will be investigated how an armature resistance, which varies with temperature, affects the speed performance of the PMDC motor.

2. Dynamic Model of PMDC Motor

The electrical equivalent model of the PMDC motor is shown in Fig. 1. (SALIM et al., 2013).

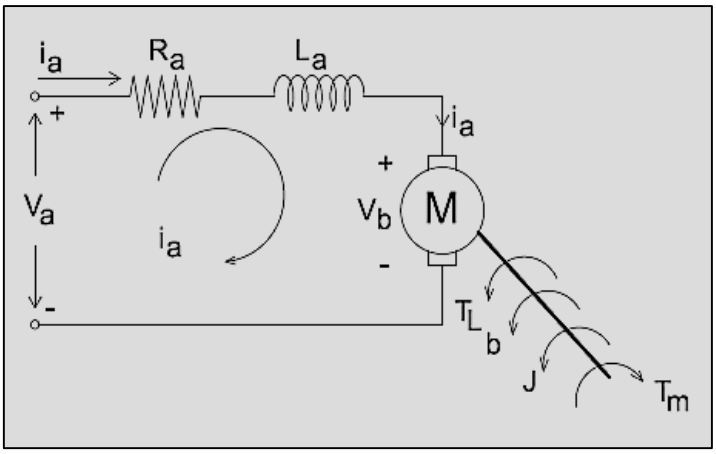

Figure 1. The electrical model of PMDC motor

From the dynamic equations of DC motor following equations are obtained by Kirchhoff Voltage Law,

$$V_a(t) = R_a i_a(t) + L_a \frac{d}{dt} i_a(t) + V_b(t) \quad (1)$$

$$V_b(t) = K_e \omega_r(t) \quad (2)$$

$$\frac{d}{dt} i_a(t) = -\frac{R_a}{L_a} i_a(t) - \frac{K_e}{L_a} \omega_r(t) + \frac{1}{L_a} V_a(t) \quad (3)$$

and from the torque equations are obtained,

$$T(t) = K_m i_a(t) \quad (4)$$

$$T(t) = J \frac{d}{dt} \omega_r(t) + b\omega_r(t) + T_L \quad (5)$$

In this study, the load moment was assumed to be zero ($T_L = 0$) during the all simulations.

$$\frac{d}{dt} \omega_r(t) = \frac{K_m}{J} i_a(t) - \frac{b}{J} \omega_r(t) \quad (6)$$

Parameters of the DC motor are given in Table 1.

Symbol	Explanation	Units	Value
b	Viscous friction	Nms	0.02
J	Inertia moment	$kg.m^2$	0.0243
K_e, K_m	Motor Constant	V.s/rad	0.125
L_a	Armature Inductance	H	0.25
R_a	Armature Resistance	Ω	3.54

Table 1. Parameters of DC motor

The simulation model of the DC motor using Eq. 3 and Eq. 6 is given in Fig. 2.

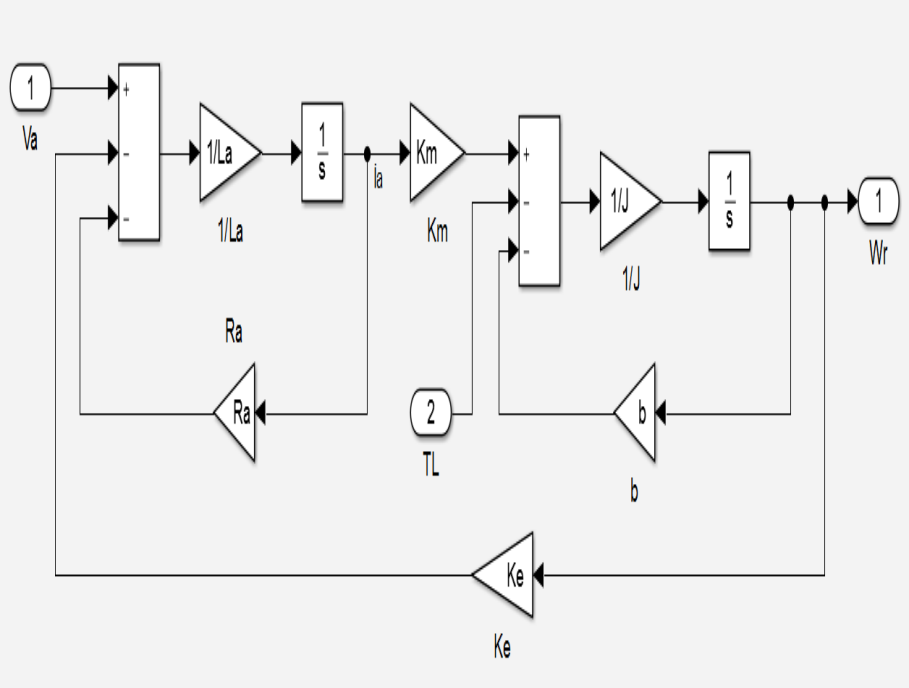

Figure 2. Simulink model of DC motor

As a result, Matlab/SIMULINK model of the DC motor without controller is shown in Fig. 3.

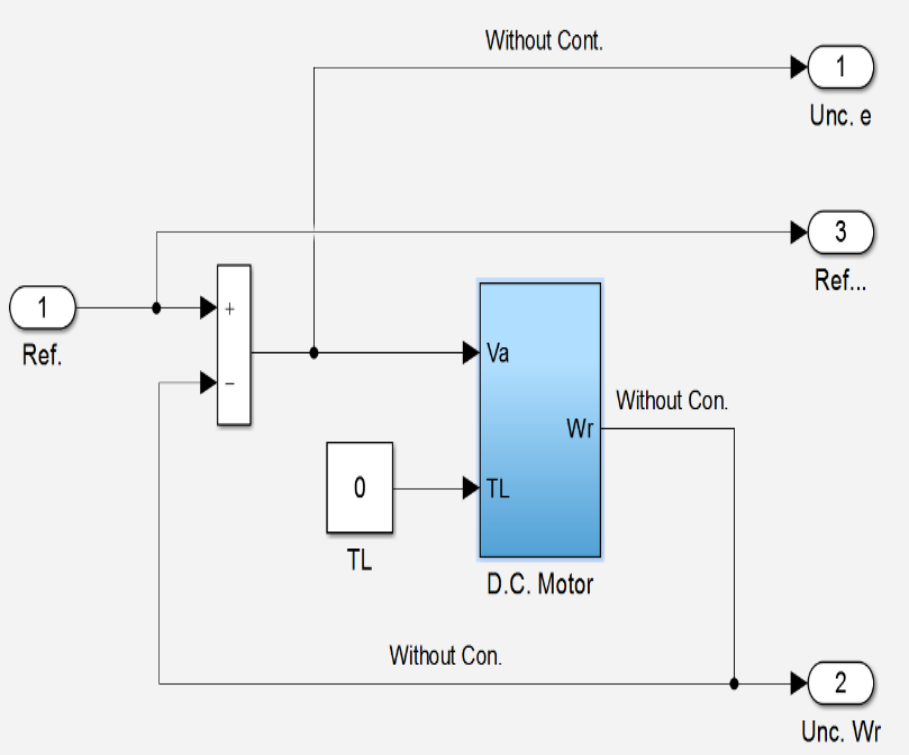

Figure 3. DC motor model without controller

As shown in Fig. 3, the load moment was assumed to be zero. The rotor angular velocity was compared with the given reference input. Firstly, the angular of 100 (rad/s) was applied for reference input. Secondly, this value was increased to 150 (rad/s) in the fifth seconds of the simulation. Finally, it was decreased to 100 (rad/s) again in the tenth seconds of the simulation. The obtained system output is shown in Fig. 4.

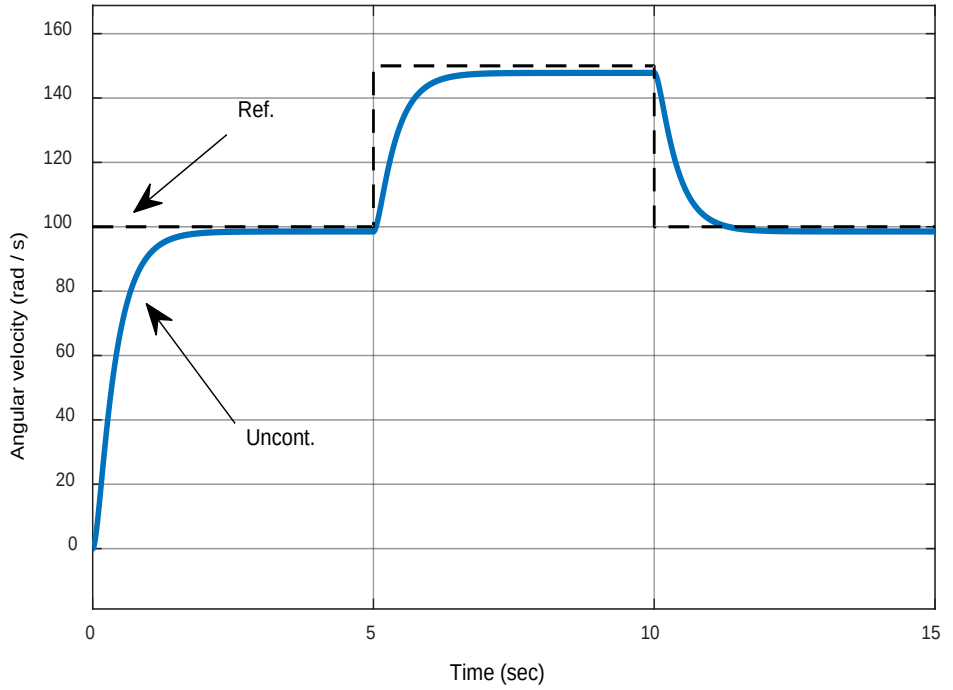

Figure 4. The DC motor speed without controller

According to Fig. 4, when the system is operated without the controller, the rotor angular velocity has not reached the given reference input values and permanent state error has occurred for each different speed references.

3. Controllers

3.1 PI Controller

PI controllers are often used in control applications due to their simple structures. In scientific studies, it is a very common control structure especially in the comparison of different control systems. In this study, was not given detailed information about the PI controller since the FL controller structure was examined. The Matlab/SIMULINK model of a simple PI controller structure is shown in Fig. 5.

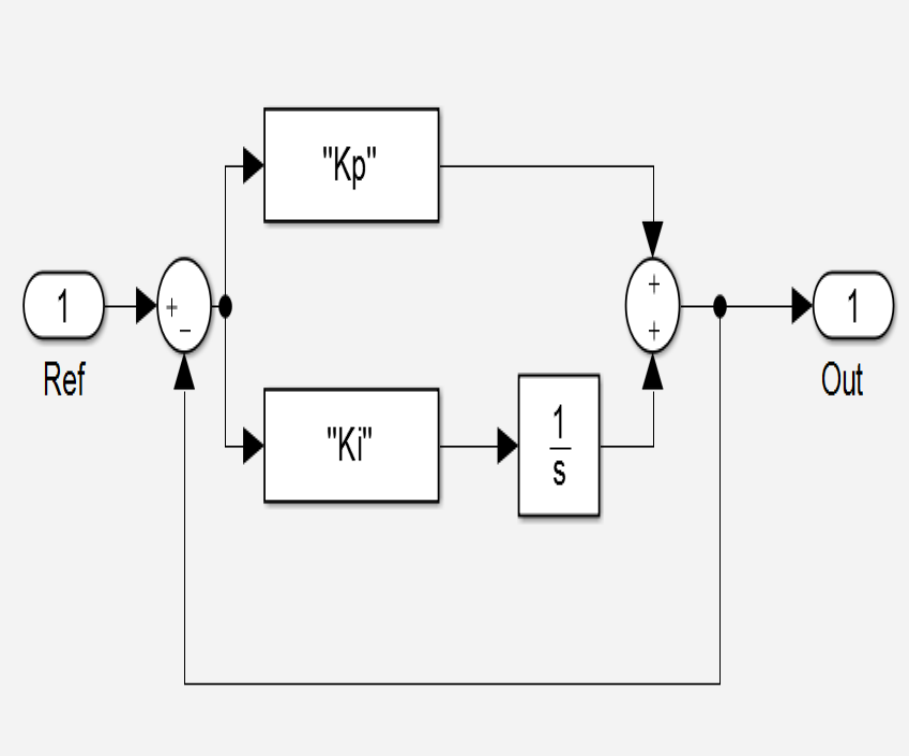

Figure 5. PI controller structure

Where Kp and Ki is proportional gain and integral gain, respectively. In this study, Kp = 1.983 and Ki = 1.969 are selected with Matlab/Tuner. PI controller for the control of DC motor was designed in Matlab/SIMULINK environment is shown in Fig. 6. Angular velocity of the rotor is shown in Fig. 7.

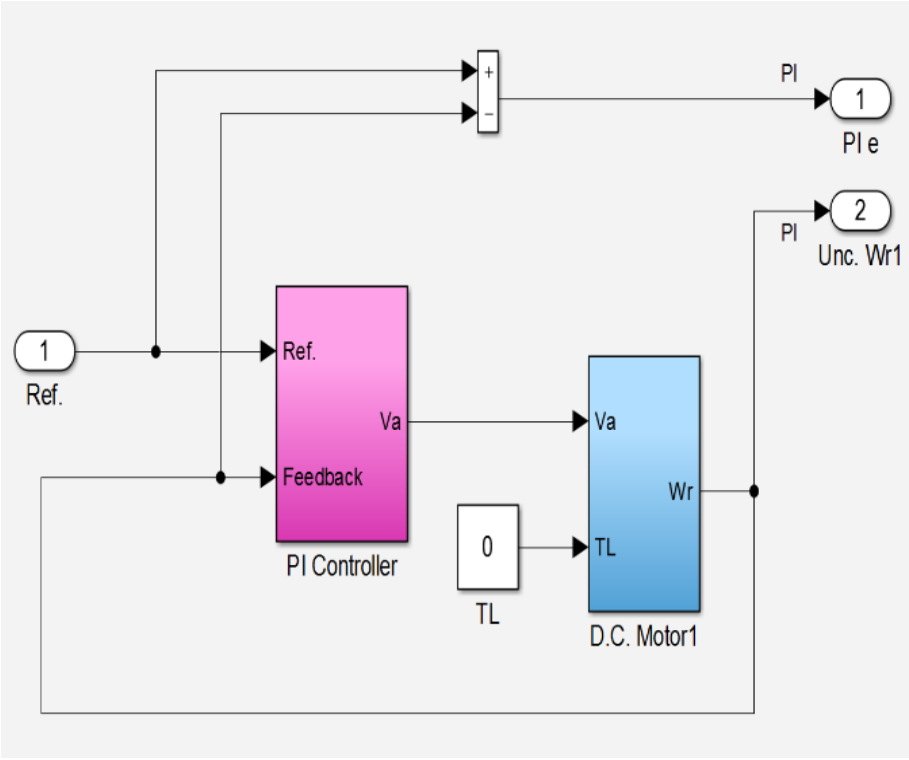

Figure 6. PI controller system

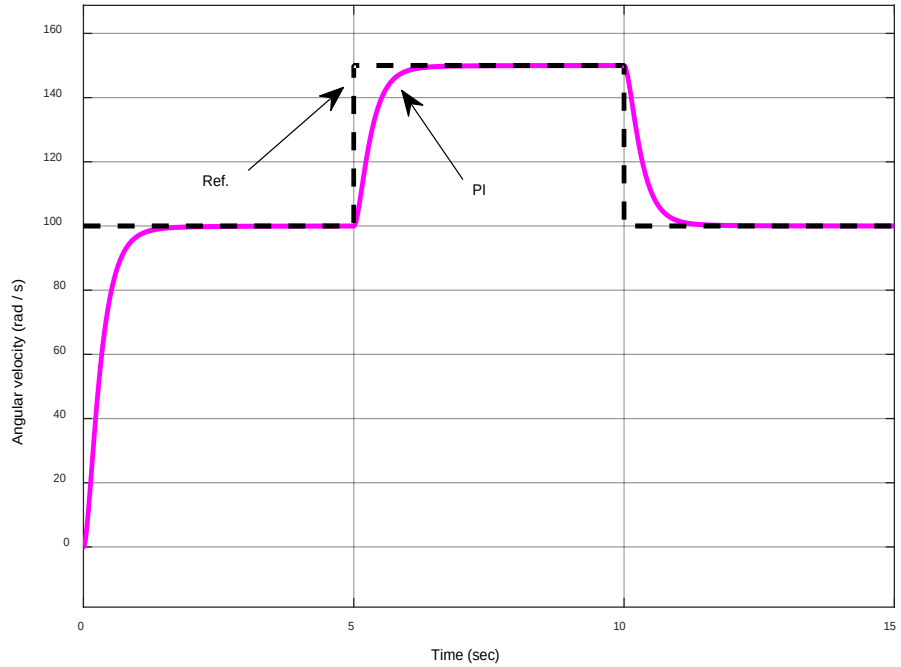

Figure 7. Angular velocity of the rotor with PI controller

3.2 Fuzzy Logic Controller

To design controller of a system, is necessary a mathematical model of that system. It is difficult to obtain mathematical models of nonlinear and uncertain systems. However, fuzzy control defines systems with complex mathematical models and numerical solutions in terms of linguistic variables. Fuzzy logic theory was first introduced by Zadeh (ZADEH, 1965). Later, in his other works about fuzzy logic, he explained that fuzzy logic can be applied to systems with uncertainty and detailed mathematical models (ALTAŞ, 1999). Zadeh (1965) has contributed greatly to the scientific world with a new control method for controlling complex systems.

Mamdani and his colleagues implemented the application for the first time of fuzzy logic theory to control systems (ALTAŞ, 1999). In this work, Matlab/SIMULINK - Fuzzy Logic Toolbox is used for fuzzy logic controller. In addition, Mamdani's fuzzy modeling is chosen for fuzzy modeling.

Additionally, Altaş et al., (2007) designed a direct fuzzy logic controller without using the Fuzzy Logic Toolbox in his published article in 2007 and implemented it to various systems (ALTAŞ, 2007; ALTAŞ, 2008).

The fuzzy logic controller consists of a number of subunits. These are called fuzzification, data base, rule base and defuzzification. The basic block diagram of the fuzzy logic controller is shown in Fig. 8.

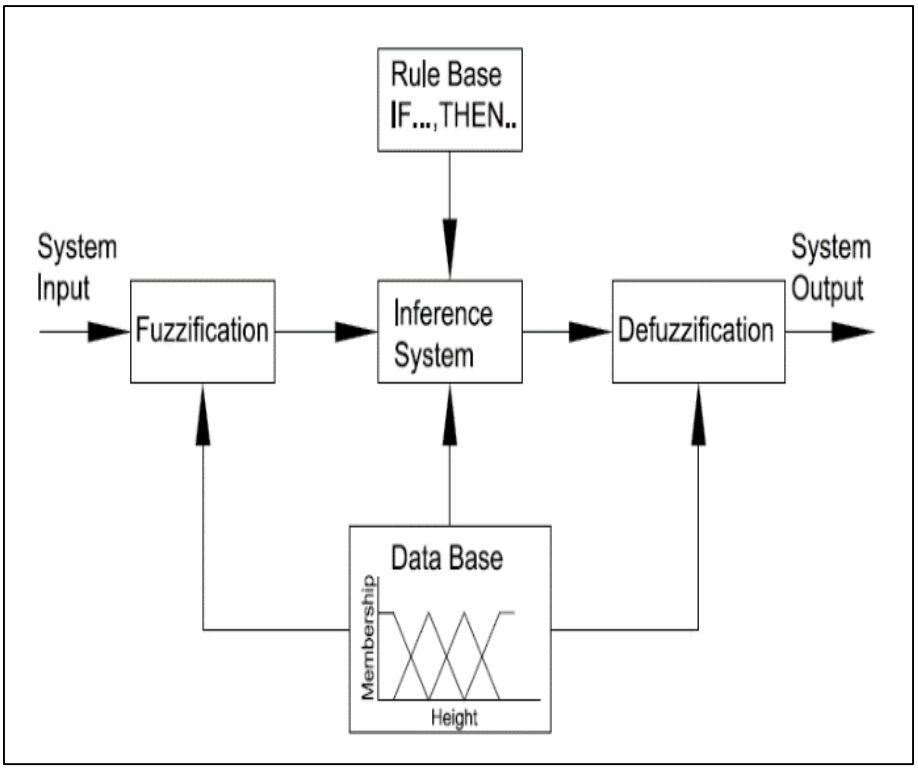

Figure 8. Blocks diagram of FLC structure.

In this study, a fuzzy logic controller with five membership functions was designed for PMDC motor control (MALLA, 2012). Although there are a large number of membership functions for fuzzy controllers, the triangle membership function was used for this study. The membership functions is shown in Fig. 9.

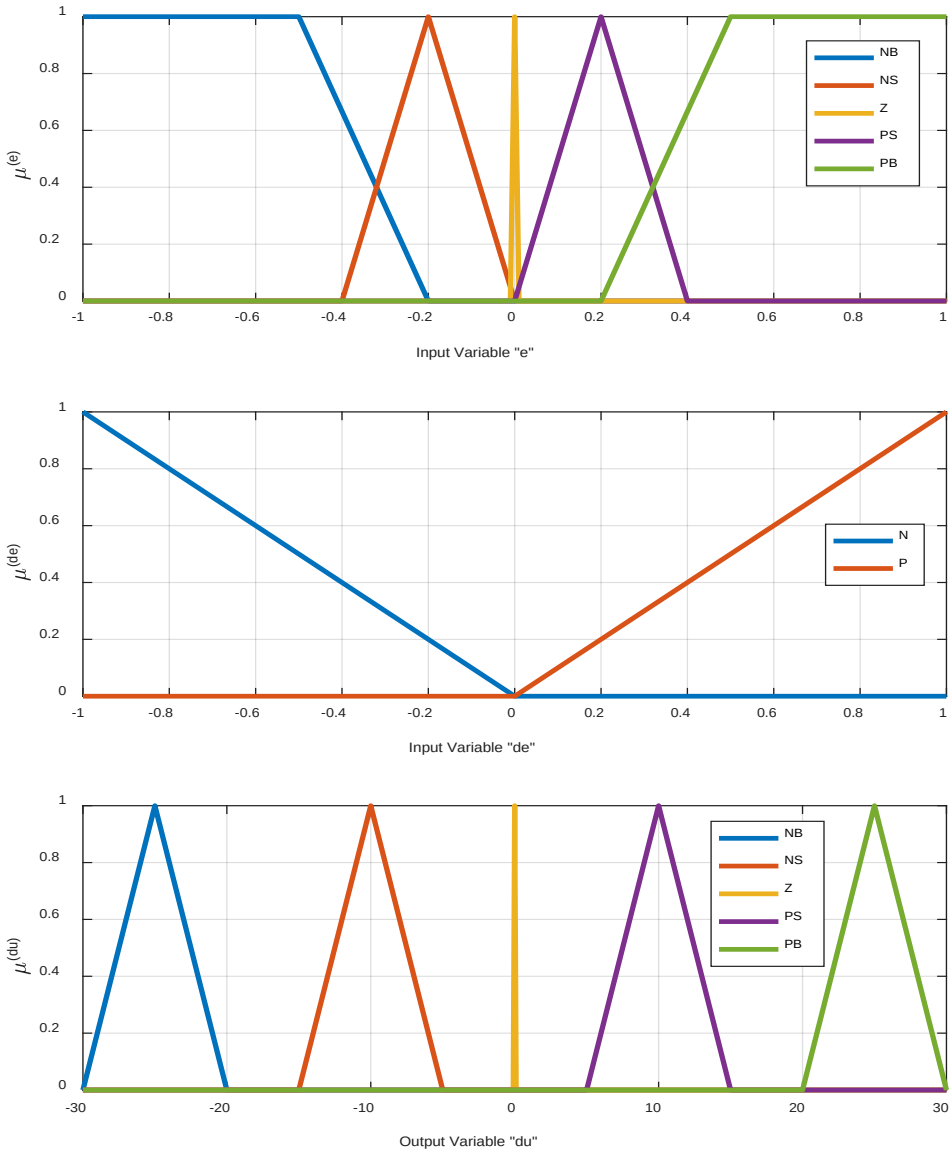

Figure 9. Membership functions of error, change of error and output

After the membership functions were determined, the rule base was created. The rule base for membership functions is given in Table 2. Where, NB: Negative Big, NS: Negative Small, Z: Zero, PS: Positive Small, PB: Positive Big.

du		e				
		NB	NS	Z	PS	PB
de	N			NS		
	P			PS		
	none	NB	NS	Z	PS	PB

Table 2. Rule Base

The system model that provides control of the dc motor with the fuzzy logic controller is shown in Fig. 10.

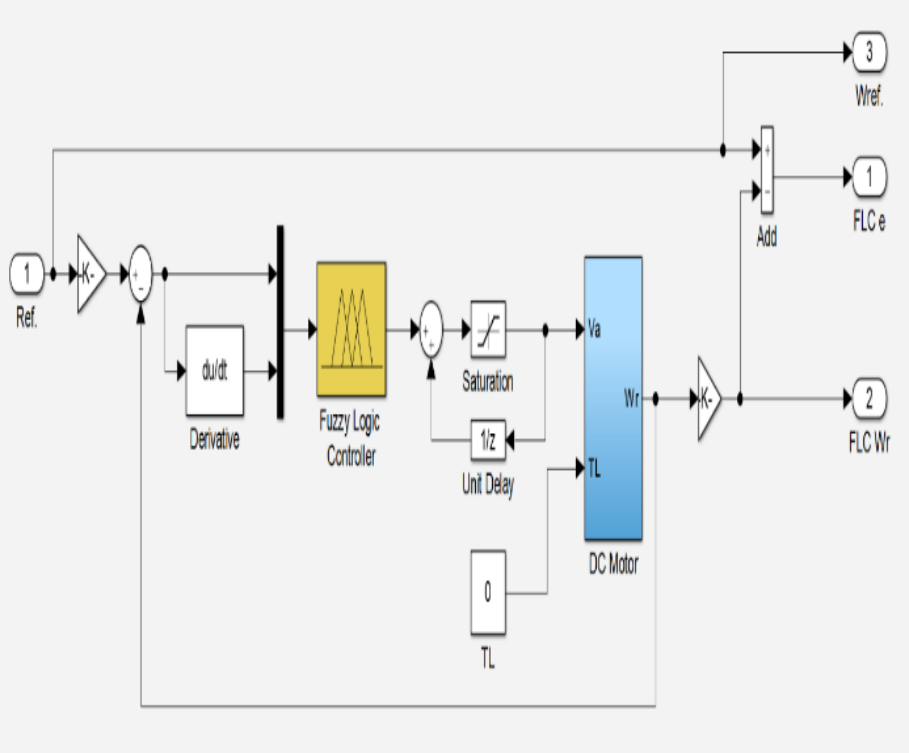

Figure 10. FL controller system

An anti-windup integrator was used at the output of the FL controller to prevent the steady state error (AÇIKGÖZ, ŞEKKELİ, 2013). The rotor angular velocity obtained using the FL controller is shown in Fig. 11.

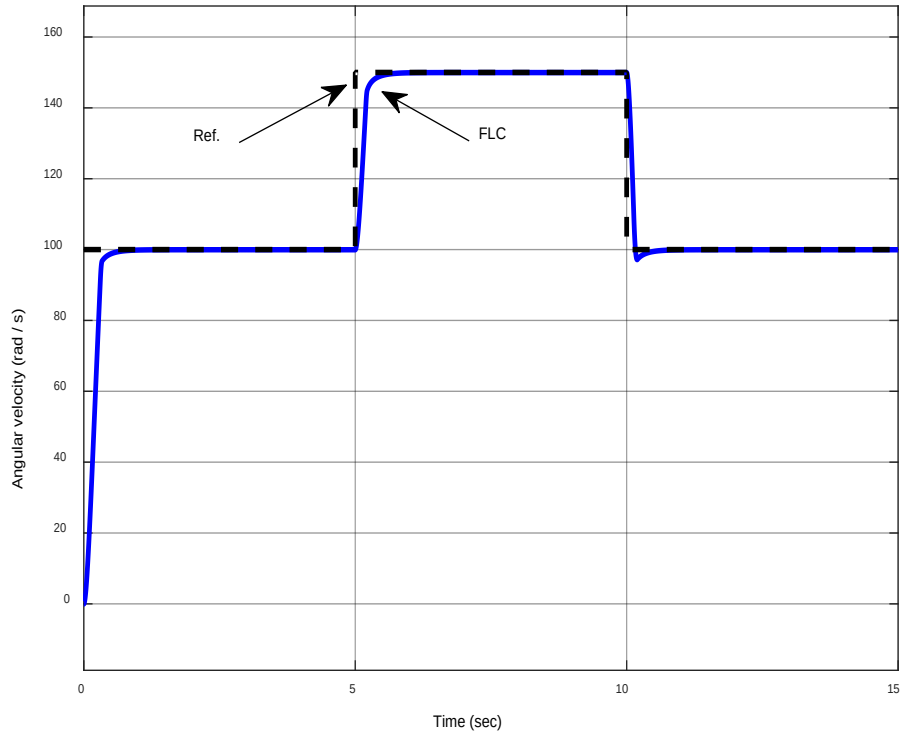

Figure 11. Angular velocity of the rotor with FL controller

4. Results and discussion

Firstly, simulation model was designed by using dynamic model of DC motor. Secondly, the speed performance analysis of the DC motor was performed with PI and FL controllers for various speed references. After these operations, the armature resistance of the DC motor was changed and the output was monitored in order to investigate the effect of different armature resistance values on the DC motor speed and controllers. To compare the data obtained, all systems were designed in a single simulation environment. The simulation model and system outputs is shown in Fig. 12, Fig. 13, respectively.

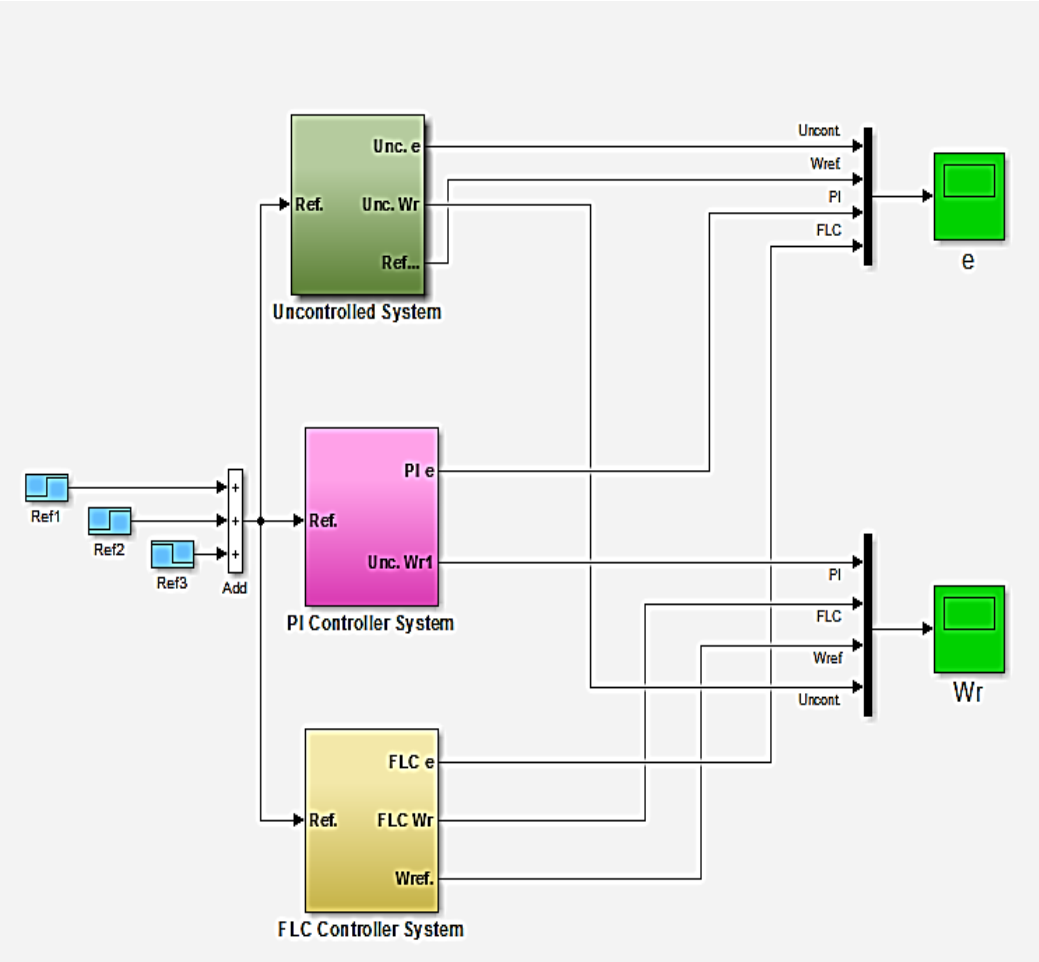

Figure 12. Simulation of all systems

As shown in Fig. 13, the best controller for variable speed references is the fuzzy logic controller. It is observed that the steady state error is zero for both controllers. However, the fuzzy logic controller has performed better than the PI controller in terms of rise time and settling time.

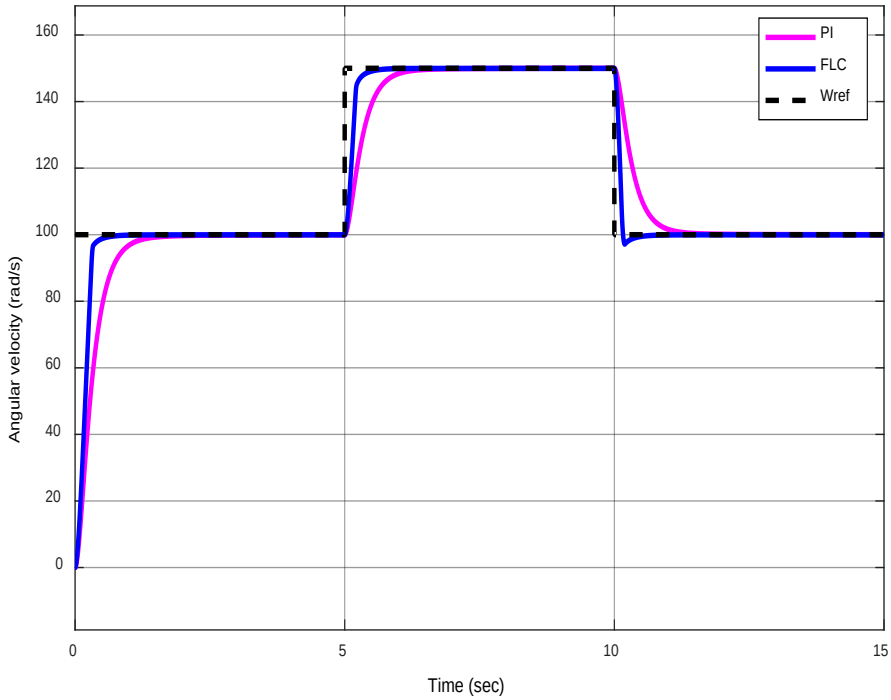

Figure 13. The angular velocity of all systems

The system outputs, when, the armature resistance increased is shown in Fig. 14. It was observed that the angular velocity of the DC motor without the controller is decreased when the armature resistance is increased. When the effect of this process on controller structures is examined, there is no effective change. The steady state error in both controllers is zero. However, increase of armature resistance was delayed rise time and settling time.

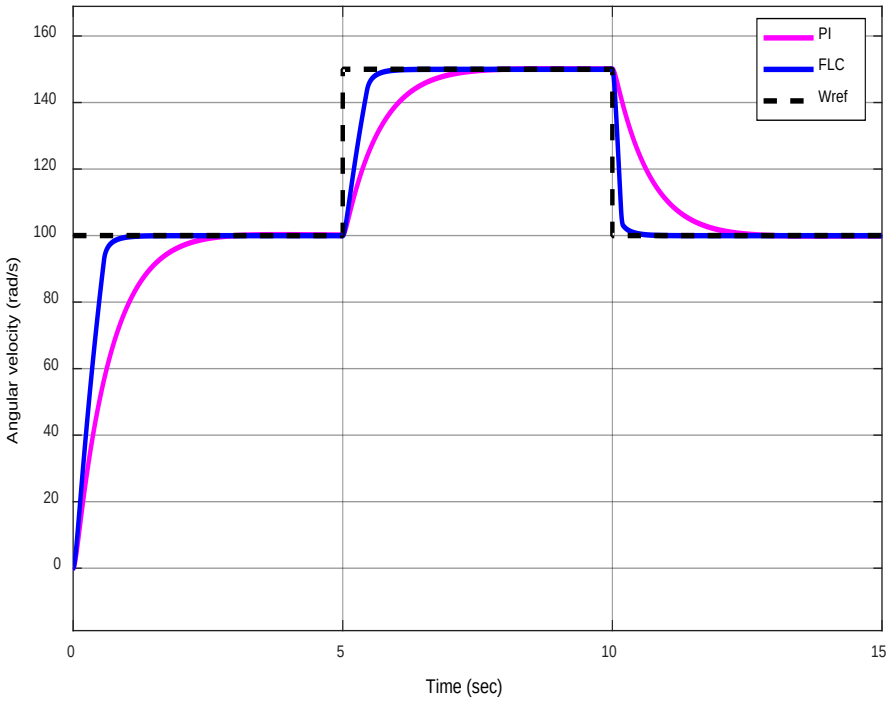

Figure 14. The angular velocity of all systems when 2*R_a

The system outputs, when, the armature resistance decreased is shown in Fig. 15. It was observed that the angular velocity of the DC motor without the controller increased when the armature resistance was decreased. As shown in Fig. 15, when the effect of this process on controller structures was examined, it has shown that while the armature resistance decreases, both controllers follow the references speeds after a small overshoot.

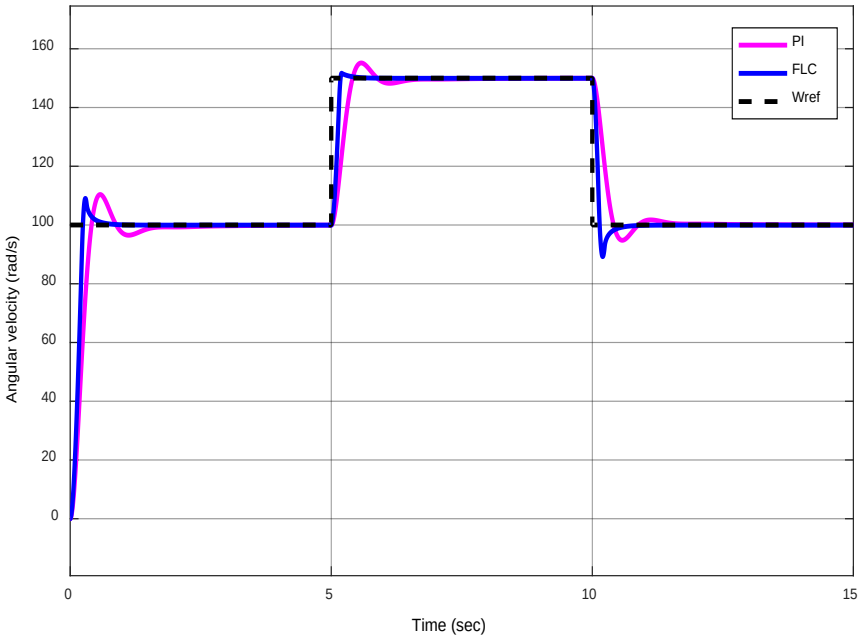

Figure 15. The angular velocity of all systems when $R_a/2$

When the DC motor is running, the resistance of the armature windings that became heated due to brush and commutator contact and friction increases by a certain amount. This heat is also related the environment temperature. Increasing the environment temperature increases the armature resistance by causing the armature windings to get warmer. As shown in Fig.14, the increase in armature resistance causes negative effects for all systems. It was observed that both controllers tracked the reference speeds with a delayed settling time. As shown in Fig.15, the decrease in armature resistance has caused the system an overshoot.

5. Conclusion

In this study, firstly, was designed a dynamic model of DC motor and modeled in Matlab/SIMULINK environment. The obtained model was run directly and the output was observed. Then, PI and FL controller structures were designed and performance analysis of the controllers were compared on the DC motor, respectively. The comparison process was performed with different speed references and different armature resistance values. According to the results on Table 3, the FL controller were provided better performance for both variable speed references and variable armature resistances than the PI controller.

System	***Ra = 3,54 Ω***		***Ra = (3,54*2) Ω***		***Ra=(3,54*0,5) Ω***	
	PI	***FLC***	***PI***	***FLC***	***PI***	***FLC***
Settling Time (s)	1.579	0.567	2.55	0.919	2.132	0.73
Rise Time (s)	0.698	0.302	1.442	0.546	0.353	0.22
Steady State Error (rad/s)	0	0	0	0	0	0
Overshoot (%)	0	0	0	0	7.9	5.2

Table 3. Output value of all systems

References

ABUZEID M. R., SHTAWA N. E., *Comparative Speed Control Study Using PID and Fuzzy Logic Controller*, International Journal of Computer Science and Electronics Engineering (IJCSEE) Volume 2, Issue 2 (2014) ISSN 2320–4028 (Online).

AÇIKGÖZ H., ŞEKKELİ M., *Bulanık Mantık Denetleyici ile Doğrudan Moment Denetim Yöntemi Uygulanan Asenkron Motorun Hız Denetim Performansının İncelenmesi*, Akademik Platform, APJES I-II, Doi:10.5505/apjes.2013.35744, 50-57, 2013.

ADEWUYI P. A., *DC Motor Speed Control: A Case between PID Controller and Fuzzy Logic Controller*, International Journal of Multidisciplinary Sciences and Engineering, Vol. 4, No. 4, May 2013.

AHMED A., MOHAN Y., CHAUHAN A., SHARMA P., *Comparative Study of Speed Control of D.C. Motor Using PI, IP, and Fuzzy Controller*, International Journal of Advanced Research in Computer and Communication Engineering Vol. 2, Issue 7, July 2013.

AHMED H., SINGH G., BHARDWAJ V., SAURAV S., AGARWAL S., *Controlling of D.C. Motor using Fuzzy Logic Controller*, Conference on Advances in Communication and Control Systems 2013 (CAC2S 2013).

AKYAZI Ö., ZENK H., AKPINAR A. S., *Farklı Bulanık Üyelik Fonksiyonları Kullanarak Sürekli Mıknatıslı DA Motorunun Hız Denetiminin Gerçeklenmesi*, 6th International Advanced Technologies Symposium (IATS'11), 16-18 May 2011, Elazığ, Turkey.

ALTAŞ İ. H., *Bulanık Mantık : Bulanık Denetim*, Enerji, Elektrik, Elektromekanik-3e, Sayı 64, Sayfalar:76-81, Bilesim Yayıncılık A.Ş., İstanbul, 1999.

ALTAŞ İ. H., *Bulanık Mantık : Bulanıklık Kavramı*, Enerji, Elektrik, Elektromekanik-3e, Sayı 62, Sayfalar:80-85, Bileşim Yayıncılık A.Ş., İstanbul, 1999.

ALTAŞ İ. H., *Bulanık Mantık Denetleyici: MATLAB/Simulink Ortamı İçin Bir Modelleme*, Otomasyon, Mart, p:158-162, 2007.

ALTAŞ İ. H., MENGI O. Ö., *Fuzzy logic control for a wind/battery renewable energy production system*, Turk J Elec Eng & Comp Sci, Vol.20, No.2, 2012.

ALTAS I. H., SHARAF A. M., *A Generalized Direct Approach for Designing Fuzzy Logic Controllers in MATLAB/Simulink GUI Environment*, International Journal of Information Technology and Intelligent Computing, Int. J. IT&IC no.4 vol.1, January 2007.

ALTAS I. H., SHARAF A. M., *A Novel GUI Modeled Fuzzy Logic Controller for a Solar Powered Energy Utilization Scheme*, The 13th International Conference on Emerging Nuclear Energy Systems (ICENES2007), June 3-8, 2007.

ARDA M., GÜLLÜ A., KUŞÇU H., *Bulanık Mantık Yönteminin PID Denetleyici Performansına Etkisi*, 16. Ulusal Makina Teorisi Sempozyumu, Atatürk Üniversitesi, Mühendislik Fakültesi, 12-13 Eylül, 2013.

BANSAL U. K., NARVEY R., *Speed Control of DC Motor Using Fuzzy PID Controller*, Advance in Electronic and Electric Engineering. ISSN 2231-1297, Volume 3, Number 9 (2013), pp. 1209-1220.

DEWANGAN K., SHUKLA S., YADU V., *Speed Control of a Separately Excited DC Motor Using Fuzzy Logic Control Based on Matlab Simulation Program*, International Journal of Scientific & Technology Research Volume 1, Issue 2, March 2012.

ISMAIL M. A. R., HEESSAIN E. M., *Speed Control of PMDC Motor using PID Controller*, International Journal of Science and Research (IJSR) ISSN (Online): 2319-7064 Index Copernicus Value (2013).

KUO B. C., *Otomatik Kontrol Sistemleri*, 7. Baskı, Literatür Yayıncılık, İstanbul, 1999.

KUSHWAH R., WADHWANI S., *Speed Control of Separately Excited Dc Motor Using Fuzzy Logic Controller*, International Journal of Engineering Trends and Technology (IJETT) - Volume4 Issue6- June 2013.

MALLA S., *Fuzzy Controller based Speed Control of DC Motor*, www.mathworks.com, May 2012.

MOHIUDDIN M. S., ALAM M., *Performance analysis of Fuzzy logic based speed control of DC motor*, IOSR Journal of Electrical

and Electronics Engineering (IOSR-JEEE) e-ISSN: 2278-1676, p-ISSN: 2320-3331, Volume 7, Issue 4 (Sep. - Oct. 2013), PP 17-24, www.iosrjournals.org.

SALIM, JYOTI OHRI, NAVEEN, *Speed Control of DC Motor using Fuzzy Logic based on LabVIEW*, International Journal of Scientific and Research Publications, Volume 3, Issue 6, June 2013 1 ISSN 2250-3153.

SIVANANDAM S. N., SUMATHI S. and DEEPA S. N., *Introduction to Fuzzy Logic using MATLAB*, ISBN-13 978-3-540-35780-3.

THORAT A. A., YADAV. SUHAS, PATIL. S. S., *Implementation of Fuzzy Logic System for DC motor Speed Control using Microcontroller*, International Journal of Engineering Research and Applications (IJERA) ISSN: 2248-9622 www.ijera.com Vol. 3, Issue 2, March -April 2013, pp.950-956.

TIWARI A., DUBEY S. P., *Performance Analysis of Fuzzy based DC Motor Drive*, International Journal of Engineering Science and Innovative Technology (IJESIT) Volume 2, Issue 2, March 2013.

YÜKSEL İ., *Otomatik Kontrol Sistem Dinamiği ve Denetim Sistemleri, Matlab ile Genişletilmiş 6. Baskı*, Nobel Yayın Dağıtım, Ankara, 2009.

ZADEH L. A., *Fuzzy Sets*, Informatıon and Control, Volume 8, Issue 3, June 1965, Pages 338-353.

Chemometric Analysis of Moxifloxacin and Metronidazole in Binary Drug Combinations With Spectrophotometric Method

GÜZİDE PEKCAN ERTOKUŞ, ÜMİT MURAT ÇELİK

Department of Chemistry Faculty of Science & Art, Süleyman Demirel University, Isparta, Turkey

Abstract

In this study, sensitive and accurate spectrophotometric-chemometric methods were developed for metronidazole and moxifloxacin without any separation step in pharmaceutical tablets. The used chemometric methods are partial least squares regression (PLS) and principal component regression (PCR). PLS and PCR were successfully applied for chemometric analysis of metronidazole and moxifloxacin in synthetic mixtures and pharmaceutical tablets. A concentration set including binary mixtures of metronidazole and moxifloxacin formed to 24 different combinations were randomly prepared in 0.1 M HCl. The accuracy and precision of the developed method were validated by analyzing synthetic mixtures containing the examined drugs. As a result of the determination, high recoveries and low standard deviations were found. Absorbance and concentration values were used in Minitab and other chemometric programs to calculate estimated concentrations with PCR and PLS. The second step, in drug tablets (Avelox and Flagy), was calculated amounts for metronidazole and moxifloxacin.

Keywords: Metronidazole and moxifloxacin, PLS, PCR.

1. Introduction

Metronidazole; 2-methyl-5-nitroimidazol-1-etanol is used as an antiprotozoal, antiamebic and antibacterial drug [1]. But metronidazole in high concentration can not eradicate all bacteria from carious lesions [2]. Metronidazole was examined spectrophotometric method [3,4], chromatographic method [5,6] and voltametric method [7,8].

Moxifloxacin; 1-cyclopropyl-7-[2,8-diazobicyclo (4.3.0) nonane]-6-fluoro-8-methoxy-1.4-dihydro-4-oxo-3-quinolone carboxylic acid [9] has a methoxy function at the 8-position and an S,S configured diazobicyclononyl ring moiety at the 7-position [10]. Moxifloxacin is enhanced activity in vitro against Gram-positive bacteria and maintenance of activity against Gram-negative bacteria [9]. Metronidazole was examined spectrophotometric method [11,12,13,14,15], chromatographic method [16,17,18] and voltametric method [19], fluorescence [20], capillary zone electrophoresis [21].

Chemometric calibration methods are observed that it is the best techniques to determinate the amount of each component in the complex mixture. The most accepted chemometric methods in drug analysis are principal component regression (PCR) and partial least squares regression (PLS) [22]. A relationship to be established between matrices of chemical data is determinated at chemometric methods [23].

In this study, principal component regression (PCR) and partial least squares regression (PLS) were successfully performed to simultaneous determination of metronidazole and moxifloxacin in a commercial tablet formulation, tablets without any separation method. Mean recoveries (%) and standard deviation of principal component regression (PCR) and partial least squares regression (PLS) methods were calculated for the validation of the methods. The acquired results were statistically compared each other.

2. Experimental

Chemicals and Reagents : All materials used were analytical grade. 0.025 g / 250 ml metronidazole 0.025 g / 250 ml moxifloxacin stock solutions were made up with 0.1 M HCl. Mixtures were prepared at various ratios. A training set and validation set containing the drugs in various proportions, 24 synthetic mixtures synthetic mixtures (for validation) was made.

Received: 10.10.2017
Revised: 02.11.2017
Accepted: 11.11.2017
Corresponding author: Güzide Pekcan Ertokuş, PhD
Department of Chemistry, Faculty of Science & Art, Süleyman Demirel University, Isparta, Turkey
E-mail: guzideertokus@sdu.edu.tr
Cite this article as: G. P. Ertokuş and Ü. M. Çelik, Chemometric Analysis of Moxifloxacin and Metronidazole in Binary Drug Combinations with Spectrophotometric Method, Eastern Anatolian Journal of Science, Vol. 3, Issue 2, 30-27, 2017.

Instruments and Software : A Shimadzu UV-1700 PharmaSpec Spectrophotometer connected to an IBM PS with UV Probe Software was used for all measurements and data processing. A pair of 1.0 cm quartz cuvettes were used for absorbance measurements.

Absorbance Measurements: Interval corresponding to the difference 0.5 between 200-500 nm were recorded for the active ingredients of the absorbance spectra. Calibration matrix and training verification sets contain two component mixtures that are optimized at different ratios. Spectra analysis of pure agents and PLS and PCR were used to calculate the concentrations.

Samples of 5-35 ppm (either alone or in combination) between the active substances were taken up into 25 ml volumetric flask volumes and completed with 0.1 M HCl. The mixtures were agitated for thorough mixing.

Procedure for real sample: For this purpose, the active substance samples were transferred to 25 ml flasks and mechanically mixed in 0.1 M HCl in a medium similar to the stomach environment.

Chemometric Method: Partial least squares regression (PLS-regression) is the most commonly used chemometric multivariate calibration method [24].

PLS is done using both experimental (or x) and concentration (or c) data simultaneously. Usually PLS is presented in the form of equations. There are a few ways to express them, the most suitable for our purpose being:

$$X = T.P. + E \quad (1)$$

$$c = T.q + f \quad (2)$$

Where X refers to the experimental measurements (e.g. spectra) and c is the concentration. There is a correlation with an installation for vector vector q. Matrix T is common to both equations. E is an error matrix and error to prevent the x vector c to block scores f orthogonal, but non-orthogonal (P) loads, generally are non-normalized [25].

The Minitab 17 program (İnova, Ankara, Turkey) was used for the analysis of all the concentration and absorbance data and to do the statistical calculations. Minitab is a statistical analysis software. In addition to statistical research, statistics can be used to learn [27].

3. Results and Discussion

Figure 1 shows the absorbance-wave length (nm) curves. The spectrum of metronidazole and moxifloxacin is in the range of 200-500 nm.

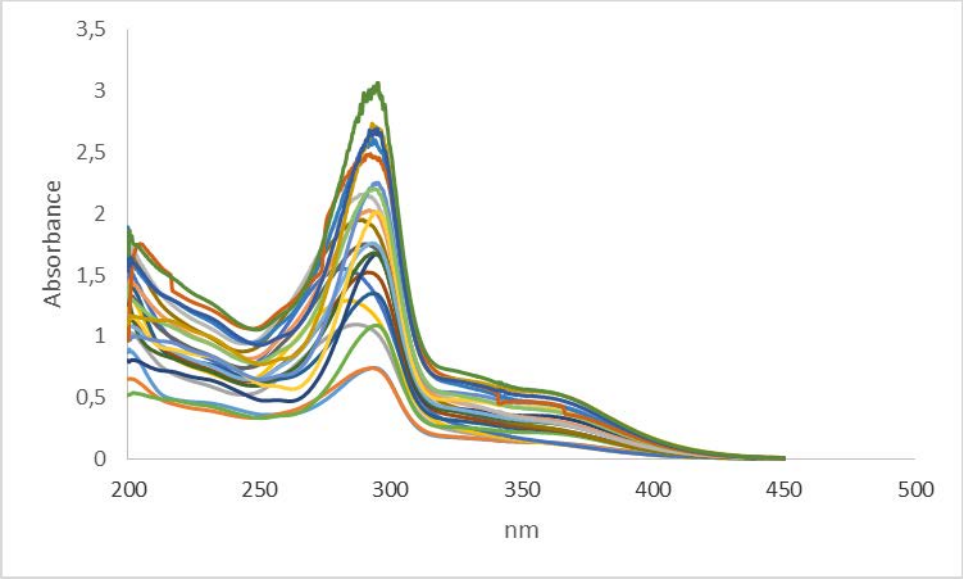

FIG. 1: The Absorption Spectrum of Metronidazole and Moxifloxacin

Fig.1 shows absorption spectra for metronidazole and moxifloxacin and their binary mixture in 0.1 M HCl.

Our objective in this study is to develop a lower-cost but more quick and reliable analytical method using chemometry. With this method, active ingredients can be analyzed without pre-separation, and loss of time and work due to the trial and error method will be prevented.

With the spectrophotometric-chemometric method used, the pharmaceutical industry will be faster and less costly. As a result, drug prices can be lowered so people can buy drugs more cheaply.

The PLS method and absorption spectra can be used individually or overlapping for multiple simultaneous detection of very linear components.

Concentrations of metronidazole and moxifloxacin mixtures are listed in Table 1. Prediction of the calibration methods was done by resolution of ten synthetic mixtures in a working concentration range for food colorants. Predicted concentration data of metronidazole and moxifloxacin mixtures is shown in Table 2. The percentage recovered and relative standard deviations are also listed in Table 2. The training set of 24 standard mixture solutions contain different concentrations of metronidazole and moxifloxacin.

Table 1: Concentratıon Set Containing Metronidazole and Moxifloxacin Compounds for The Preparation of The Pcr and Pls Calibration.

No	Moxifloxacin ppm	Metronidazole ppm
1	5	7
2	5	14
3	5	21
4	5	28
5	5	35
6	10	7
7	10	14
8	10	21
9	10	28
10	10	35
11	15	7
12	15	14
13	15	21
14	15	28
15	15	35
16	20	7
17	20	14
18	20	21
19	20	28
20	20	35
21	25	7
22	25	21
23	25	28
24	25	35

Table 2 : Composition of Prediction Set and Recovery Results Obtained in Synthetic Mixtures for Pls Method

	Moxifloxacin			Metronidazole		
Mixture No	Actual (ppm)	Predicted (ppm)	% Recovery	Actual (ppm)	Predicted (ppm)	% Recovery
1	5	4.85	97.00	7	6.98	99.71
2	5	4.97	99.40	14	13.92	99.43
3	5	4.94	98.80	21	20.95	99.76
4	5	4.86	97.20	28	27.89	99.61
5	5	5.01	100.20	35	34.79	99.40
6	10	9.86	98.60	7	6.97	99.57
7	10	9.87	98.70	14	13.94	99.57
8	10	9.97	99.70	21	19.96	95.05
9	10	10.00	100.00	28	27.93	99.75
10	10	9.97	99.70	35	34.97	99.91
11	15	14.96	99.73	7	6.92	98.86
12	15	14.95	99.67	14	13.85	98.93
13	15	14.97	99.80	21	20.97	99.86
14	15	14.93	99.53	28	27.99	99.96
15	15	14.98	99.87	35	34.82	99.49
16	20	19.85	99.25	7	6.89	98.43
17	20	19.87	99.35	14	13.96	99.71
18	20	19.82	99.10	21	20.98	99.90
19	20	19.89	99.45	28	27.89	99.61
20	20	19.97	99.85	35	34.96	99.89
21	25	24.78	99.12	7	6.98	99.71
22	25	24.98	99.92	21	20.95	99.76
23	25	24.97	99.88	28	27.97	99.89
24	25	25.01	100.04	35	34.96	99.89
			Mean=99.33 **SS**=0.808			**Mean**=99.40 **SS**=0.999

Table 3: Composition of prediction set and recovery results obtained in synthetic mixtures for Pcr method

	Moxifloxacin			Metronidazole		
Mixture No	Actual (ppm)	Predicted (ppm)	% Recovery	Actual (ppm)	Predicted (ppm)	% Recovery
1	5	4.98	99.60	7	7.01	100.14
2	5	4.88	97.60	14	13.85	98.93
3	5	4.92	98.40	21	20.86	99.33
4	5	4.97	99.40	28	27.88	99.57
5	5	4.86	97.20	35	34.85	99.57
6	10	9.97	99.70	7	6.5	92.86
7	10	9.86	98.60	14	13.89	99.21
8	10	9.88	98.80	21	19.95	95.00
9	10	9.89	98.90	28	27.98	99.93
10	10	9.85	98.50	35	34.89	99.69
11	15	14.96	99.73	7	6.95	99.29
12	15	14.97	99.80	14	13.98	99.86
13	15	14.86	99.07	21	20.95	99.76
14	15	14.92	99.47	28	27.98	99.93
15	15	14.96	99.73	35	34.96	99.89
16	20	19.86	99.30	7	6.96	99.43
17	20	19.87	99.35	14	13.97	99.79
18	20	19.99	99.95	21	20.97	99.86
19	20	19.95	99.75	28	27.96	99.86
20	20	19.96	99.80	35	34.98	99.94
21	25	24.96	99.84	7	6.85	97.86
22	25	24.86	99.44	21	20.91	99.57
23	25	24.92	99.68	28	27.94	99.79
24	25	24.86	99.44	35	34.85	99.57
			Mean=99.21 **SS**=0.720			**Mean**=99.43 **SS**=0.68

This study, the statistical parameters were found to produce a satisfactory validity for the PLS and PCR methods. The PLS and PCR methods have reliable accuracy and higher precision.

For calibration the prediction residual error sum-of-squares (PRESS) was calculated as:

$$PRESS = \sum_{i=1}^{n} (C_i^{added} - C_i^{found})^2 \quad (3)$$

C_i^{added} : True Concentration, additional concentration of drug substance C_i^{added} : Estimated Concentration, calculate concentration of drug substance

Some statistical parameters determined the effectiveness of the calibration. The standard error of prediction (SEP) was calculated using the following expression:

$$SEP = \sqrt{\frac{\sum_{i=1}^{n} (C_i^{added} - C_i^{found})^2}{n-1}} \quad (4)$$

C_i^{added} : Actual Concentration, the added concentration of drug, C_i^{added} : Predicted Concentration, the calculated concentration of drug, n: the total number of synthetic mixtures

According to the actual and predicted concentrations of the samples, SEP and PRESS values of metronidazole and moxifloxacin were calculated and listed in Table 3.

Analysis of real samples: Table 4 lists the experimental results of the two numerical methods for commercial products and as you can see the obtained results are very close to each other (Avelox and Flagyl).

Table 3 : Statistical parameter values for calibration step- simultaneous determination of metronidazole and moxifloxacin using partial least square and principal component regression methods.

PARAMETER	METHOT	METRONIDAZOLE	MOXIFLOXACIN
SEP	PLS	0.036	0.025
	PCR	0.043	0.028
PRESS	PLS	0.052	0.0096
	PCR	0.064	0.0096

Table 4: Determination of metronidazole and moxifloxacin in commercial products using PLS and PCR methods.

	METRONIDAZOLE(GRAM)		MOXIFLOXACIN(GRAM)	
NO	PLS	PCR	PLS	PCR
1	0,495	0,496	0,435	0,436
2	0,49	0,492	0,436	0,434
3	0,496	0,497	0,43	0,432
4	0,497	0,493	0,432	0,435
5	0,496	0,495	0,434	0,435
Mean	0,4948	0,4946	0,4334	0,4344
Standard Deviation	0,002775	0,002074	0,002408	0,001517

In this study, chemometric methods can be applied to simultaneously measure spectra data processing based metronidazole and moxifloxacin samples containing mixtures of homogeneously mixed binary drug samples.

In order to compare the performances of the investigated chemometric techniques according to UV spectrophotometric method for real samples we applied Snedecor's *F*-test.

The method used to compare the differences between the one-way ANOVA tests was applied to real samples of the drug sample. In this study, F values of Snedecor were calculated and compared with F values (p = 0.05). The ANOVA test results for metronidazole were 0.0014 (PLS) and 0.0020 (PCR). The ANOVA test results for moxifloxacin 0.0013 (PLS) and 0.0017 (PCR). Experimental (calculated) F values did not exceed F-value (4.05) in analysis of variance. This is the result of a meaningful difference between all these methods. All statistical parameters and numerical values are suitable for real-time simultaneous identification.

4. Conclusions

The partial least squares method and the main component regression, which were successfully applied, were able to identify the active ingredients in the synthetic solutions separately. For all values, low prediction errors and high correlation coefficients emphasize the high linear relationship between predicted and actual concentrations. The results obtained with this binary mixture and some ratios of component concentrations indicate excellent prediction ability with these methods.

Acknowledgement: This research work has been supported by research grants from Süleyman Demirel University Scientific Research Project 4901-YL1-17.

References

ELKADY, E.F., MAHROUSE, M.A., (2011), *Reversed-phase ion-pair HPLC and TLC-densitometric methods for the simultaneous determination of ciprofloxacin hyrochloride and metronidazole in tablets*, Chromatographia, (73), 297-305.

TRAIRATVORAKUL, C., DETSOMBOONRAT, P., (2011), *Success rates of a mixtures of ciprofloxacin, metronidazole and minocycline antibiotics used in the non-instrumentation endodontic treatment of mandibular primary molars with carious pulpal involvement*, International Journal of Paediatric Dentistry, 1-11.

JAIN, R., JAIN, N., JAIN, D.K., PATEL, V.K., RAJAK, H., JAIN, S.K., (2017), *Novel UV spectrophotometer methods for quantitative estimation of metronidazole and furazolidone using mixed hydrotropy solubilization*, Arabian Journal of Chemistry, (10), 151-156.

MAHROUSE, M.A., ELKADY, E.F., (2011), *Validated spectrophotometric methods for the simultaneous determination of ciprofloxacin hydrochloride and metronidazole in tablets*, Chem. Pharm. Bull., 59(12), 1485-1493.

SAHOO, D.R., JAIN, S., (2016), *A rapid and validated RP-HPLC method for the simultaneous quantificiation of benzoic acid, metronidazole and miconazole nitrate in vaginal formulations*, Journal of Chromatographic Sciences, 54(9), 1613-1618.

MORCOSS, M.M., ABDELWAHAB, N.S., ALI, N.W., ELSAADY, M.T., (2016), *Different chromatographic methods for simultaneous determination of diloxanide furoate, metronidazole and its toxic impurity*, J.Iran Chem Soc, (13), 1643-1651.

HERNANDEZ-JIMENEZ, A., ROA-MORALES, G., REYES-PEREZ, H., BALDERAS-HERNANDEZ, P., BARRERA-DIAZ, C.E., BERNABE-PINEDA, M., (2016), *Voltammetric determination of metronidazole using a sensor based on electropolymerization of α-Cyclodextrin over a carbon paste electrode*, Electoanalysis, (28), 704-710.

SAGHRAVANIAN, M., EBRAHIMI, M., ES'HAGHI, Z., BEYRAMABADI, S.A., (2017), *Experimental sensing and density functional theory study of an ionic liquid mediated carbon nanotube modified carbon-paste electrode for electrochemical detection of metronidazole*, South African Journal of Chemistry,(70), 29-37.

SULTAN, M.A., (2009), *New, simple and validated kinetics spectrophotometric method for determination of moxifloxacine in its pharmaceutical formulations*, Arabian Journal of Chemistry, (2), 79-85.

AL OMARI, M.M.H., JAAFARI, D.S., AL-SOUOD, K.A., BADWAN, A.A., (2014),

Moxifloxacin Hydrochloride, Profiles of Drug Substances. Excipients and Related Methodology, (39), 299-420.

ASHOUR, S., BAYRAM, R., (2015), *Development and validation of sensitive kinetic spectrophotometric method for the determination of moxifloxacin antibiotic in püre and commercial tablets*, Spectrochimica Acta Part A: Molecular and Biomolecular Spectroscopy, (140), 216-222.

PEKAMWAR, S.S., KALYANKAR, T.M., TAMBE, B.V., WADHER, S.J., (2015), *Validated UV-Visible spectrophotometric method for simultaneous estimation of cefixime and moxifloxacin in pharmaceutical dosage form*, Journal of Applied Pharmaceutical Science, 5(01), 037-041.

GOUDA, A.A., AMIN, A.S., EL-SHEIKH, R., YUOSEF, A.G., (2014), *Spectrophotometric determination of gemifloxacin mesylate, moxifloxacin hydrochloride, and enrofloxacin in pharmaceutical formulations using acid dyes*, Journal of Analytical Methods in Chemistry, 1-16.

MOTWANI, S.K., CHOPRA, S., AHMAD, F.J., KHAR, R.K., (2007), *Validated spectrophotometric methods for the estimation of moxifloxacin in bulk and pharmaceutical formulations*, Spectrochimica Acta Part A, (68), 250-256.

ATTIMARAD, M., AL-DHUBIAB, B.E., ALHAIDER, I.A., NAIR, A.B., HARRSHA, S., AHMED, M., (2012), *Simultaneous determination of moxifloxacin and cefixime by first and ratio first derivative ultraviolet spectrophotometry*, Chemistry Central Journal, (6:105), 2-7.

DJURDJEVIC, P., CIRIC, A., DJURDJEVIC, A., STANKOV, M.J., (2009), *Optimization of separation and determination of moxifloxacin and its related substances by RP-HPLC*, Journal of Pharmaceutical and Biomedical Analysis, (50), 117-126.

RAZZAQ, S.N., ASHFAQ, M., KHAN, I.U., MARIAM, I., RAZZAQ, S.S., AZEEM, W., (2017), *Simultaneous determination of dexamethasone and moxifloxacin in pharmaceutical formulations using stability indicating HPLC method*, Arabian Journal of Chemistry, (10), 321-328.

KHAN, F.U., HASIR, F., IQBAL, Z., KHAN, I., SHAHBAZ, N., HASSAN, M., ULLAH, F., (2016), *Simultaneous determination of moxifloxacin and ofloxacin in physicological fluids using high performance liquid chromatography with ultraviolet detection*, Journal of Chromatography B, (1017-1018), 120-128.

RADI, A.E., WAHDAN, T., ANWAR, Z., MOSTAFA, H., (2010), *Electrochemical and spectroscopic studies on the interaction of gatifloxacin, moxifloxacin and sparfloxacin with DNA and their analytical applications*, Electroanalysis, (22), 2665-2671.

VOSOUGH, M., ESHLAGHI, S.N., ZADMARD, R., (2015), *On the performance of multiway methods for simultaneous quantification of two fluoroquinolones in urine samples by fluorescence spectroscopy and second-order calibration strategies*, Spectrochimica Acta Part A:Molecular and Biomolecular Spectroscopy, (136), 618-624.

FARIA, A.F., SOUZA, M.V.N., ALMEIDA, M.V., OLIVEIRA, M.A.L., (2006), *Simultaneous separation of five fluoroquinolone antibiotics by capillary zone electrophoresis*, Analytica Chimica Acta, (579), 185-192.

USTUNDAG, O., DINC, E., OZDEMIR, N., TILKAN, M.G., (2015), *Comparative application of PLS and PCR methods to simultaneous quantitative estimation and simultaneous dissolution test of zidovudine – lamivudine tablet*, Acta Chim. Slov., (62),437-444.

SANCHEZ-RODRIGUEZ M.I, SANCHEZ-LOPEZ E.M, MARINAS A, CARIDAD J.M, URBANO F.J, MARINAS J.M, (2014), *New approaches in the chemometric analysis of infrared spectra of extra-virgin olive oils*, SORT, 38(2): 231-250.

KENNETH R.B., (1997), Chemometrics: A practical guide, John Wiley & Sons. Inc., New York.

BRERETON R.C., (2007), Applied Chemometrics for Scientists, John Wiley & Sons. Inc., New York. Minitab 18 Statistical Programme http://www.inovadanismanlik.com.tr/_tu/_urunler/_minitab18/m18.html (10.10.2017)

Evaluation of Detection Limits with Wavelength Dispersive X-Ray Fluorescence Spectrometry

EBRU SENEMTAŞI ÜNAL[1], NESLİHAN EKİNCİ[2]

[1]*Department of Electricity and Energy, Ağrı İbrahim Çeçen University, Ağrı, Turkey*
[2]*Department of Physics, Faculty of Science, Atatürk University, 25240, Erzurum, Turkey*

Abstract

The influence of analyte mass concentration on the determination of detection limits has been investigated by using WDXRF (Wavelength dispersive X- ray fluorescence) spectrometry. Ti, V, Cr, Mn, Fe, Ni, Cu, Zn, As, Y, Zr, Nb, Mo, Ag, Cd, Sb, Nd, Gd, Er elements and binary and triple combination of these elements have been used. The samples have been selected considering the absorption edges due to the importance of the effect of matrix absorption and enhancement. The elements which have absorption edges that are close to each other have been used observe the matrix absorption and enhancement. From this results corresponding to the interval of 5-25 times the best value of the detection limits of analytical concentration values are found to be the ideal values. It is concluded that WDXRF spectrometry is a suitable technique for the determination of detection limits.

Keywords: analyte, detection limits, WDXRF, matrix, absorption and enhancement.

1. Introduction

X-ray fluorescence spectrometry is one of the appropriate techniques for elemental analysis of materials. This technique is based on the sample excitation with the release of the secondary X-rays. They contain a concentration of the elements in an unknown sample by comparison with standards of known values located in another sample PITSCH (2000).

Received: 29.09.2017
Revised: 26.10.2017
Accepted: 11.11.2017
Corresponding author: Ebru Senemtaşı Ünal, PhD
Department of Electricity and Energy, Ağrı İbrahim Çeçen University, Ağrı, Turkey
E-mail: esenemtasi@agri.edu.tr
Cite this article as: E. S. Ünal, N. Ekinci, Evaluation of Detection Limits with Wavelength Dispersive X-Ray Fluorescence Spectrometry, Eastern Anatolian Journal of Science, Vol. 3, Issue 2, 38-47, 2017

A commercial WDXRF (Wavelength dispersive X-ray fluorescence) spectrometer (Bruker S4 Explorer, Karlsruhe, West Germany) was used for analysis of the different samples. All the elements in the sample can be determined simultaneously in the WDXRF spectrometry. This instrument is usually equipped with a 1 kW Rh-anode tube working at a voltage range of 20-50 kV and a current from 50 to 20 mA. It is possible to use primary beam filters (made of Al or Cu) between the primary radiation and the sample holder to reduce the background continuum and to improve the signal-to-noise ratio. Energy resolution and efficiency for each analytical line also depend on the collimator aperture and the analyzer crystals in use. Detection can be performed using a flow proportional counter (light elements) or a scintillation counter (heavy elements) GONZALEZ-FERNANDEZ et al. (2009). In this work, analyses were made in vacuum atmosphere.

The detection limits, is of interest to analytical chemists due to the trace detection of the compound. In many literature, improved analytical methods used to determine the detection limit and new instruments used are mentioned. THOMPSON (1998) mentioned in his theoretical work that the limit of detection can never be fully interpreted, in fact it seems to be a very difficult subject to be understood and defined on the basis of this seemingly simple matter.

Then, CURRIE (2000) noted that despite the successful work on the detection limit, some problems still exist in this work. The problem of determining the limit of detection has been shown to occur more in biological and environmental samples. ROUSSEAU (2001) investigated the effect of analytical errors on the detection limit, using some chemical samples, and calculated how much the systematic and random error sources affected the result. In the following years TIWARI et al. (2005) investigated the effect of analyte mass concentration on the detection limit using total reflectance X-ray fluorescence (TXRF) and energy X-ray fluorescence (EDXRF) spectrometers. As a result, they observed that the analyte mass concentration affected the detection limit values. SHALTOUT et al. (2007)

determined the detection limit values by atomic absorption spectroscopy using Cd, Ni, Pb and Zn samples and showed that the detection limit value could be decreased by adjusting the absorption mode and counting time. KARJOU (2007) investigated matrix effects on the detection limit by using TXRF spectrometry using multiple standard solutions of the NH_4NO_3 sample at various concentrations. He observed that the low matrix concentration did not affect the detection limit, but the high matrix concentration strongly affected the detection limit. He also investigated the effect of sample mass on the detection limit using soil and blood samples and showed that the detection limit increased with increasing sample mass in the concentration unit but the detection limit increased with increasing sample mass in mass unit.

In studies carried out until today, the effects of matrix effects and analytical mass concentration on the detection limit have been investigated using various instruments, liquids and biological samples on the detection limit. But we know that since the detection limit is an indication of sensitivity, the most accurate analytical mass that should be used to obtain the most accurate measurement should be determined in scientific studies. In this study, a study was carried out to investigate the values of appropriate analyte concentrations and obtain more accurate results. Here, it is aimed to achieve accurate sample standards using WDXRF spectrometer.

2. Experimental Details

The detection limit is usually defined as the smallest amount of an analyte that can be detected in a specimen. However, it is often misinterpreted as the smallest concentration of an analyte that can be determined with reliability in a given sample ROUSSEAU (2001). In X-ray fluorescence measurements, its most common definition is the amount of analyte that gives a net line intensity equal to three times the square root of the background intensity for a specified counting time or the amount that gives a net intensity equal to three times the standard counting error of the background intensity. Hence, detection limit is related to the capability of instrument to distinguish peak intensity from the fluctuations of the background intensity due to counting statistics, or background noise EKINCI et al. (2013) (Furthermore, the detection limit calculations are based on background measurements, which are below any peak intensity used for a possible determination.

The following formula is commonly accepted to define the detection limit in XRF techniques VAN GRIEKEN (1993) and KLOCKENKAMPER (1997),

$$C_{DL} = \frac{3}{S\left(\frac{N_B}{T}\right)^{1/2}} \qquad (1)$$

Where C_{DL} is the detection limit (mass or concentration unit), N_B is the intensity of the background under the respective peak in count per second (cps), S is the sensitivity (net peak counts per second, per mass or concentration unit and T is the counting time (s). The equation shows that increasing S and T, and reducing N_B improves the C_{DL}.

Mathematically, as per the IUPAC recommendation, the detection limit has been defined in terms of standard counting error of the background intensity BERTIN (1975). If σ_p and σ_b are the counting errors of the individual peak and the background, respectively, then the Standard counting error for a net count can be expressed as,

$$\sigma = \sqrt{{\sigma_p}^2 + {\sigma_b}^2}$$

In the limit of detection one can assume $\sigma_b \approx \sigma_p$. Therefore

$$\sigma = \sqrt{2\sigma_b}$$

For 95% confidence level, the counting error would be

$$2\sigma = 3\sigma_b = 3\sqrt{N_B}$$

By taking into account the counting time T and the slope m of fluorescence intensity vs. analyte concentration curve one can write the expression for minimum detectable concentration for an analyte element as

$$C_{DL} = \frac{3}{m}\sqrt{\frac{N_B}{T}}$$

or

$$C_{DL} = \frac{3\sqrt{I_b}}{\frac{I_A}{C_A}}, \quad m = {I_A}/{C_A} \qquad (2)$$

Where I_b= background intensity (N_B/T); I_A= net area intensity; C_A= mass concentration of analyte; N_B=

background counts in a given time T; m= I_A/C_A, i.e. slope of analyte counts concentration curve; C_{DL}= minimum detectable concentration of analyte. From Eq. (2), it is clear that, for a specified counting time, the minimum detectable concentration of analyte or detection limit depends mainly on two parameters: the background intensity I_b and the net area intensity per unit analyte mass (I_A/C_A) TIWARI (2005).

XRF is often studied in solid samples. However, analysis of the solution can be performed using a suitable apparatus. Solid samples or adjusting surface sample is irradiated directly or tablet then made into a powder before irradiation. Sample will be considered in the preparation to ensure homogeneity biggest point is. Quick and simple way to prepare powder is directly pressed into the pallets of equal density. Samples were irradiated by placing the cell sample prepared by the method of assembly.

In this study, ZSX 1000e wavelength X-ray fluorescence device produced by Rigaku Company was used. In the WDXRF spectrometer, the analyzer crystal distributes the secondary characteristic X-ray so that each wavelength can be measured separately.

X-ray fluorescence spectroscopy usually involves working with solid samples. However, the analysis of the solutions can also be carried out using appropriate tool. The solid samples are either irradiated directly by smoothing a surface such as in steel analysis, or first powdered and then tableted and irradiated. The greatest point to note in preparing the sample is to ensure homogeneity. If the sample is in the form of very fine powder or if it can be crumbled to the grain size below 200 mesh, the powder sample is mixed with the necessary materials and then pressed into a tablet.

Analytical information for long wave length will be generated when well powdered powders are pressed at high pressure. Powders can be pressed into aluminum containers and steel circles. Alternatively, a boric acid binder or a hard pressing binder may be used.

In this study, samples have been selected considering the absorption edges due to the effect of matrix absorption and enhancement. The elements which have absorption edges that are close to each other have been used observe the matrix absorption and enhancement. Ti, V, Cr, Mn, Fe, Ni, Cu, Zn, As, Y, Zr, Nb, Mo, Ag, Cd, Sb, Nd, Gd, Er elements and binary and triple combination of these elements have been used. A total of 69 samples were prepared, including the pure substance and mixtures. Mixtures to study the effect on the detection limit of the concentration of analyte and matrix were prepared at different concentrations. Powdered samples were first milled using an agate mortar and then sieved through 100-400 mesh fine sieves to remove particle size effect. Then all the pressed samples were prepared in the same form with a thickness of 13 mm by applying a pressure of 10 tons equally to each sample with a pressing machine. Any losses that might occur during sample preparation and error to minimize tools are used. Samples were prepared in the form of pellets of mass 0.6g. The advantage of making these pellets is that interelement enhancement effects in the sample are minimized. Counting time for each sample has been set 10800s. Manufactured by Rigaku Company ZSX 1000e WDXRF instrument was used. The data received by the WDXRF system is transferred to the origin pro 7.5 of the program and element spectra have been drawn. Representatively, the spectrum of 0.6g Cr sample is showed in Fig 1.

Detection limits of the elements were calculated from using Eq (2). Calculated results are shown in the table 1, table 2, table 3, table 4 and table 5.

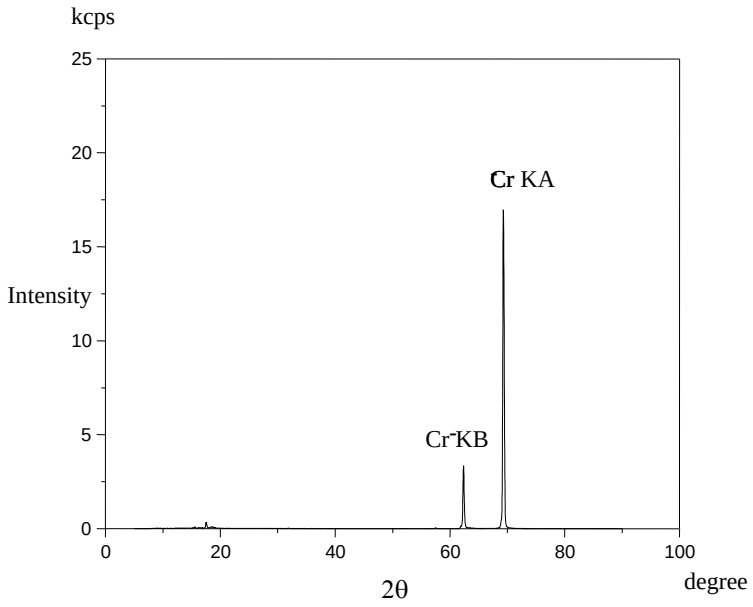

Figure 1. 0.6g Cr sample of X-ray spectrum of K_α and K_β.

Table 1. The C_{DL} has been calculated for Ti, Cr, V elements and binary and triple combination of these elements.

Sample	Analyte	C_{DL} (ppm)
Ti		8,21683
Cr		6,24160
V		5,71532
0,5Ti 0,1V		
	Ti	6,18057
	V	1,34397
0,4Ti 0,2V		
	Ti	5,05238
	V	2,19541
0,3Ti 0,3V		
	Ti	4,89362
	V	2,95654
0,5V 0,1Cr		
	V	5,55337
	Cr	1,09310
0,4V 0,2Cr		
	V	5,04408
0,3V 0,3Cr	Cr	1,43912
	V	4,63893
	Cr	2,61159
0,5Ti 0,1Cr		
	Ti	7,83066
	Cr	0, 80172
0,4Ti 0,2Cr		
	Ti	5,51336
	Cr	2,22325
0,3Ti0,3Cr		
	Ti	4,82093
	Cr	3,08829

0,4Ti 0,1V 0,1Cr	Ti	3, 92613
	V	1,17492
	Cr	2,13014
0,3Ti 0,2V 0,1Cr	Ti	3,24820
	V	2,22665
	Cr	1,28536
0,3Mn 0,1Fe 0,2Ni	Ti	2,83310
	V	2,31355
	Cr	1,45261
0,2Mn 0,2Fe 0,2Ni	Ti	2,50904
	V	1,64086
	Cr	2,56115

Table 2. The C_{DL} has been calculated for As, Y, Zr, Nb, Mo elements.

Sample	**C_{DL} (ppm)**
As	5,15022
Y	7,35368
Zr	7,50342
Nb	7,94702
Mo	8,02405

Table 3. The C_{DL} has been calculated for Fe, Mn, Ni elements and binary and triple combination of these elements.

Sample	**Analyte**	**C_{DL} (ppm)**
Fe		5,69786
Mn		5,26947
Ni		5,14553
0,5Mn 0,1Fe		
	Mn	3,14869
	Fe	0,38061
0,4Mn 0,2Fe		
	Mn	4,62920
	Fe	0,55162
0,3Mn 0,3Fe		
	Mn	4,93372
	Fe	2,16401
0,5Mn 0,1Ni		
	Mn	3,64869
	Ni	2,96533
0,4Mn 0,2Ni		
	Mn	2,72444
0,3Mn 0,3Ni	Ni	4,14291
	Mn	2,17375
	Ni	5,40387
0,5Fe 0,1Ni		
	Fe	5,38086
	Ni	1, 74123
0,4Fe 0,2Ni		

	Fe	4,79443
	Ni	2,37291
0,3Fe 0,3Ni		
	Fe	4,19142
	Ni	4,61387
0,4Mn 0,1Fe 0,1Ni	Mn	3, 61961
	Fe	0,24320
	Ni	1,65356
0,3Mn 0,2Fe 0,1Ni	Mn	2,84615
	Fe	0,61279
	Ni	1,81125
0,3Mn 0,1Fe 0,2Ni	Mn	2,14044
	Fe	0,25263
	Ni	2,78491
0,2Mn 0,2Fe 0,2Ni	Mn	1,88106
	Fe	0,51117
	Ni	2,82660

Table 4. The C_{DL} has been calculated for Ag, Cd, Sb elements and binary and triple combination of these elements.

Sample	**Analyte**	**C_{DL} (ppm)**
Ag		8,12247
Cd		9,22396
Sb		10,0217
0,5Ag0,1Cd		
	Ag	7,65784
	Cd	0,54496
0,4Ag0,2Cd		
	Ag	6,44775
	Cd	1,82913
0,3Ag0,3Cd		
	Ag	3,92228
	Cd	4,78321
0,5Cd0,1Sb		
	Cd	7,78526
	Sb	1,58377
0,4Cd0,2Sb		
	Cd	6,41392
	Sb	3,04778
0,3Cd0,3Sb		
	Cd	4,93237
	Sb	4,61682
0,5Ag 0,1Sb		
	Ag	5,75317
	Sb	1,93770
0,4Ag0,2Sb		
	Ag	4,72392
	Sb	2,94944
0,3Ag0,3Sb		
	Ag	3,90539
	Sb	4,85898
0,4Ag0,1Cd0,1Sb		

	Ag	5,52481
	Cd	1,26692
	Sb	1,68731
0,3Ag 0,2Cd 0,1Sb		
	Ag	5,03097
	Cd	2,35657
	Sb	1,71835
0,3Ag 0,1Cd 0,2Sb		
	Ag	4,61418
	Cd	1,51606
	Sb	2,84283
0,2Ag 0,2Cd 0,2Sb		
	Ag	3,25696
	Cd	2,43185
	Sb	3,21256

Table 5. The C_{DL} has been calculated for Nd, Er, Sb elements and binary and triple combination of these elements.

Sample	**Analyte**	**C_{DL} (ppm)**
Nd		15,1860
Gd		17,8293
Er		18,6608
0,5Nd0.1Gd		
	Nd	14,1688
	Gd	1,26718
0,4Nd0,2Gd		
	Nd	12,2619
	Gd	3,64456
0,3Nd0,3Gd		
	Nd	1,12522
	Gd	16,2169
0,5Gd0,1Er		
	Gd	16,0117
	Er	1,89313
0,4Gd0,2Er		
	Gd	13,9736
	Er	4,17825
0,3Gd0,3Er		
	Gd	9,84345
	Er	9,14732
0,5Nd 0,1Er		
	Nd	10,0412
	Er	3,65477
0,4Nd 0,2Er		
	Nd	9,31480
	Er	6,24224
0,3Nd 0,3Er		
	Nd	5,87458
	Er	9,56043
0,4Nd 0,1Gd 0,1Er		

	Nd	11,2636
	Gd	1,05750
	Er	2,03146
0,3Nd 0,2Gd 0,1Er		
	Nd	11,1478
	Gd	3,51325
	Er	2,58146
0,3Nd 0,1Gd 0,2Er		
	Nd	9,65643
	Gd	1,27062
	Er	2,62759
0,2Nd 0,2Gd 0,2Er		
	Nd	2,17820
	Gd	4,45414
	Er	9,15146

4. Result and Discussion

In this study, mixtures of various ratios of elements on the C_{DL} are used to observe the effects of matrix. To investigate the analyte mass concentration on detection limits, in the present study, Ti, V, Cr, Mn, Fe, Ni, Cu, Zn, As, Y, Zr, Nb, Mo, Ag, Cd, Sb, Nd, Gd, Er elements and binary and triple combination of these elements were chosen as test samples. Tables 1, 2, 3, 4 and 5 demonstrate the detection limit values of these samples. As a result, it was found that the detection limit for the low analyte concentration was more affected than the high analyte concentration. If the analyte concentration is reduced, the background significantly decreases as the fluorescence peak increases the tail width. Decreasing the analyte concentration causes the analyte peak to weaken and causes the detection limit value to be smaller than the appropriate value.

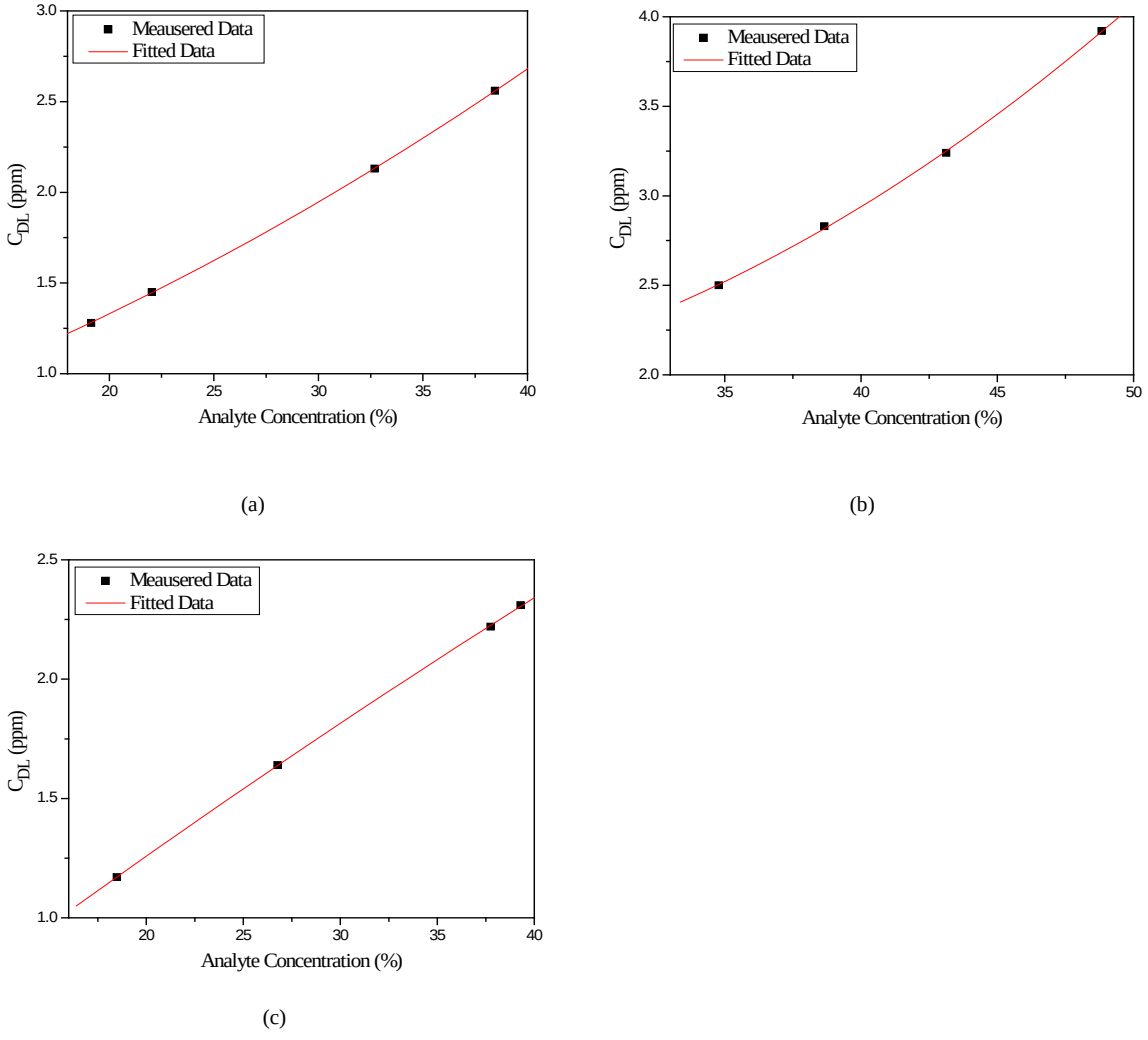

Figure 2. (a) Variation of Ti detection limits with analyte concentration in the sample of TiVCr. (b) Variation of V detection limits with analyte concentration in the sample of TiVCr. (c) Variation of Cr detection limits with analyte concentration in the sample of TiVCr.

As shown in figure 2 (a) drawn for the TiVCr sample, the minimum detectable limit for Ti analysis is equal to the analyte concentration of 2,509 ppm to 34,78 ppm (about 14 times). As shown in Figure 2 (b), the minimum detectable limit value for V analytics is equal to the analyte concentration of 1,175 ppm to 18,48 ppm (about 16 times). As shown in Figure 2 (b), the minimum detection limit for Cr analysis is equal to the analyte concentration of 1,285 ppm to 19,13 ppm (about 15 times).

We have also taken into account the total errors contributed in detection limits measurement as well as in preparation of analyte concentration. Since the detection limit depends linearly on analyte concentration, the net error in these two parameters has been calculated partially. The total error contributed to detection limit measurement has been found to vary from 1-8%.

One of the biggest problems encountered in XRF analyzes is the matrix absorption enhancement effects. The intensity of the secondary X-ray given by the quantitative element is influenced by the other elements in the sample, either positively or negatively. As a result of this influence, the analyte intensity may be greater or less than predicted. For the K lines of consecutive element pairs from the periodic table atomic number 22 titanium to the atomic number 72 hafnium from the atomic order, absorption-enhancing effects occur at the middle level. In this study, if the atomic number of Ti is 22, the atomic number of 23 is V, and the atomic number of 24 is Cr, For the TiV mixture, K_α of the V excites the Ti. For the VCr mixture, K_α of the Cr excites the V. For the TiCr mixture, K_α of the Cr excites the Ti. For the TiVCr mixture, K_α of the V excites the Ti, K_α of the Cr excites Ti, K_α of the Cr excites V and K_α of the V excites Ti The contributions to the intensity of Ti from the primary beam excitation are directly enhancement by the K_α of V, direct enhancement by the K_α of Cr and the third element enhancement by the K_α of V. All of the angular spectrometers and devices that select the pulse height cannot distinguish these lines. For this reason, the K_α and K_β lines of some elements are overlaid.

In conclusion, our study shows that the detection limit tends to be dependent on the analyte concentration. The results from this systematic study are given in order to get the best detection limit value under the experimental conditions that can help us on what should be required of the mass concentration of the analyte. The results obtained indicate that the optimum value of detection limit will correspond to analyte mass concentration 5-25 times of the best detection limit. It is clear from this that the limit of detection is dependent on the analyte mass concentration.

References

BERTIN, E. P. (1975), *Principles and practice of X-ray spectrometric analysis*, David Sarnoff Research Center, 1079 p, New York and London. Conference in Kristiansand vom, Haan.

CURIE, L. (2000), *Detection and quantification capabilities and the evaluation of low-level data: some international perspectives and continuing challenges*. Journal of Radioanalytical and Nuclear Chemistry, 245(1), 145-156.

EKINCI, R., EKINCI, N., and SENEMTAŞI, E. (2013). *Effect of analysis time on detection limit by energy dispersive X-ray fluorescence spectrometry*, Asian Journal of Chemistry, vol. 25, No. 5, 2557-2560.

GONZALEZ-FERNANDEZ, O., MARGUI, E., and QUERALT, I. (2009). *Multielemental analysis of dried residue from metal-bearing waters by wavelength dispersive X-ray fluorescence spectrometry*. Spectrochimica Acta Part B*:* Atomic Spectroscopy, 64(2), 184-190.

KARJOU, J. (2007), *Matrix effect on dedection limit and accuracy in total reflection X-rayflourescence analysis of trace elements in environmental and biological samples*. Spectrochima Acta Part B, 62(2), 177–181.

KLOCKENKAMPER., R. (1997), *Total-Reflection X-Ray Fluorescence Analysis*, vol. 140, J. Wiley and Sons, Inc, New York, pp. 173-214.

PITSCH, H. (2000), *The preparation of samples of solid substances for spectroscopic analysis,* 11th Norwegian X-ray Conference in Kristians and vom, Haan.

PITSCH, H. (2000), *The preparation of samples of solid substances for spectroscopic analysis,* 11th Norwegian X-ray

ROUSSEAU, R. M. (2001), *Detection limits and estimates of uncertainity of analytical XRF results*, The Rigaku Journal, 18 (2), 33–47.

SHALTOUT, A. A., and IBRAHIM, M. A. (2007), *Detection limit enhancement of Cd, Ni, Pb and Zn determined by flame atomic absorption spectroscopy*. National Research Center, 52(5),276-286.

THOMPSON, M. (1998), *Do we really need detection limits.* The Analyst, 123, 405–407.

TIWARI, M. K., SINGH, A. K., SAWHNEY, J.S. (2005), *Sample preparation for evaluation of X-ray flourescence spectrometry*, Analytical Sciences, 21 (2), 143–147.

VAN GRIEKEN., R. E., A. MARKOWICZ. (1993), Handbook of X-ray spectrometry: Methods and Techniques, vol. 14, M. Dekker, Inc, New York, pp. 453-489.

.